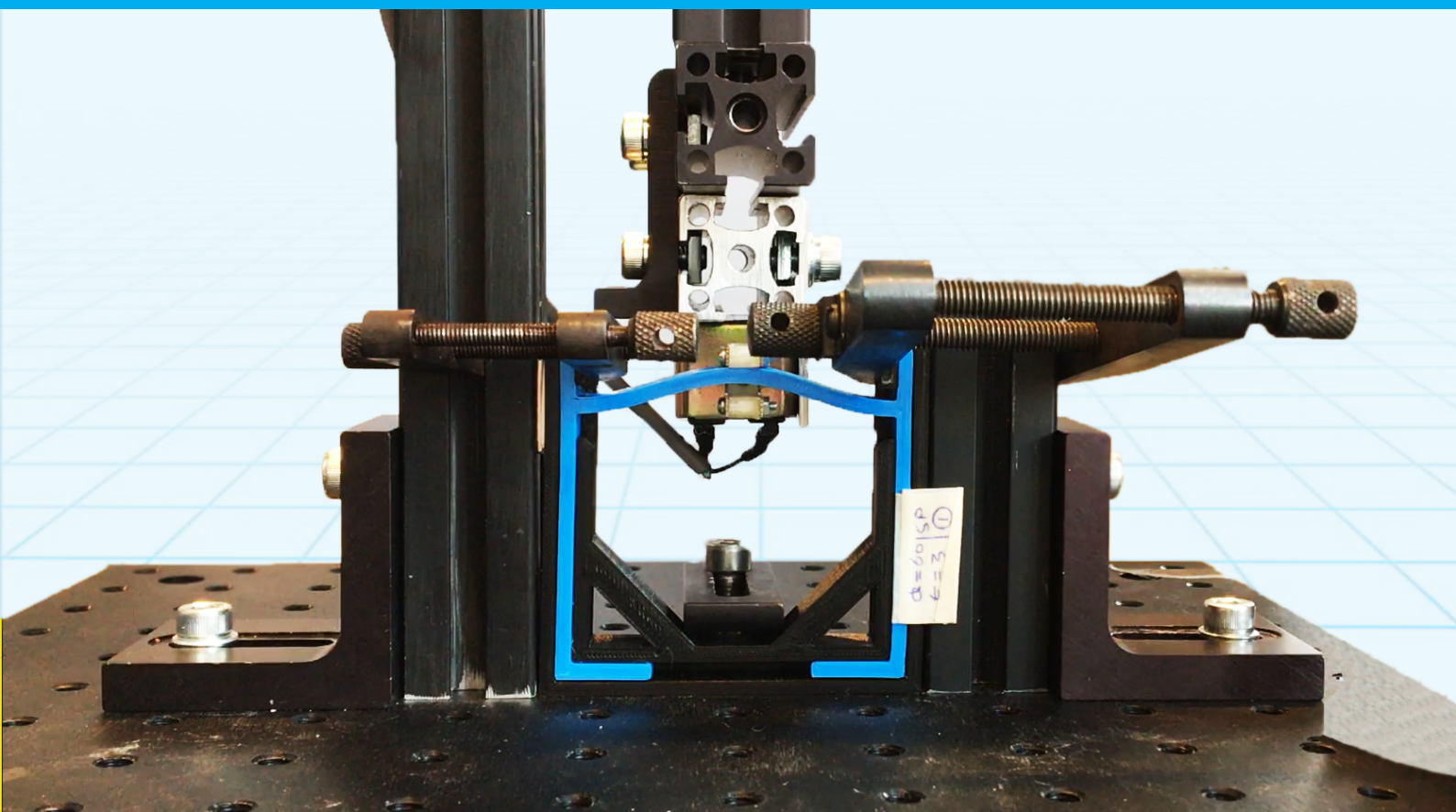


# Modelling of Metastable Equilibrium State using PRB Principles

Krishna Dheeraj Kommuri





# Modelling of Metastable Equilibrium State using PRB Principles

by

Krishna Dheeraj Kommuri

to obtain the degree of Master of Science  
at the Delft University of Technology,  
to be defended publicly on Monday November 25, 2019 at 09:00 AM.

Student number: 4734173  
Project duration: February 12, 2019 – November 24, 2019  
Thesis committee: Prof. dr. ir. J. L. Herder, TU Delft, supervisor  
Dr. ir. G. Smit, TU Delft, supervisor  
F. G. J. Broeren Msc, TU Delft, supervisor  
Dr.ir. M. Aguirre, Milton Medical B. V.

An electronic version of this thesis is available at <http://repository.tudelft.nl/>.





# Preface

August of 2017 was my first visit to the Netherlands, ever since then the TU Delft community has created a nourishing environment for me to thrive. I am grateful for all the opportunities and support provided by the university. I would like to take this opportunity to thank Milton Aguirre for offering me an internship at Milton Medical and taking an interest in my career. Our occasional trips to the cheese store and teaching the intricacy in apple tasting are some of the many experiences I will cherish.

I would also like to thank Freek Broeren for his interest in my thesis. Freek has created an excellent environment for me to improve, he was respectful of my learning pace and offered his suggestions when needed. I am forever grateful for Freeks understanding of my plan and for his help to meet them. I would like to thank Just Herder and Gerwin Smit for their involvement in my thesis. Their academic and administrative support were of great value.

I am thankful for the support offered by Patrick van Holst and Bradly But in realising my thesis. Patricks advice has helped fill the voids in the literature, his knowledge and problem-solving skills helped me meet the experimental challenge with ease. I am thankful for Bradlys help in fixing my printer and for his support in building tools needed for the experiment.

My journey to the Netherlands was only possible, thanks to my parents, my brother and his family. Their constant enquiry on my well-being has left me humble. Their clueless excitement at my work is heartwarming and appreciable. I am grateful for their support, and forever be indebted to their generosity.

I would like to take time in thanking Hemanth, Srujan, Rohit and Karthik for their endless calls and being there for me when needed. I would also like to thank my friends Sushanth, Sindhuja, Marcelo, Luo, Maria, Julia, Rahul, Sanjit, Prajish, Jay, Aneesh and Ashwin for making my Delft experience memorable.

Krishna Dheeraj Kommuri  
Delft, November 2019



# Contents

<b>1</b>	<b>Introduction</b>	<b>1</b>
<b>2</b>	<b>Literature review: Classifying Bistable systems and Identifying a feasible bistable system that can be redesigned for metastability</b>	<b>3</b>
<b>3</b>	<b>Modelling of Metastable Equilibrium State using PRB Principles</b>	<b>13</b>
<b>4</b>	<b>Discussion</b>	<b>27</b>
<b>5</b>	<b>Conclusion</b>	<b>29</b>
<b>A</b>	<b>Appendix: 3D printer settings</b>	<b>31</b>
<b>B</b>	<b>Appendix: SLS Model Behaviour</b>	<b>33</b>
	B.1 SLS Transfer Function Modelling . . . . .	33
	B.2 Force response for Constant deformation. . . . .	34
	B.3 Recovery Time estimation . . . . .	35
<b>C</b>	<b>Appendix: PRB Model selection</b>	<b>37</b>
	C.1 Appendix: PRB model design . . . . .	37
<b>D</b>	<b>Appendix: Material Test</b>	<b>41</b>
	D.1 Bending Test . . . . .	41
	D.2 Tensile Test . . . . .	43
	D.3 Compression Test . . . . .	43
<b>E</b>	<b>Appendix: Matlab Script</b>	<b>45</b>
	<b>Bibliography</b>	<b>59</b>



# Introduction

This thesis focuses on modelling a metastable equilibrium state in pre-curved beams. The bases of the focus start with the literature study of metamaterials. The field of metamaterials is an intriguing branch of engineering with an ability to alter properties like Poissons ratio [15] energy absorption [16] and many more with the help of the geometric structures. Katia Bertoldis [6] work on classification has helped understand various forms of metamaterials.

Although many properties can be fabricated using metamaterials, the literature study followed in this thesis only focused on the study of metamaterials with bistable unit cell structure(fundamental repeating structure of metamaterial). The results of the literature study have revealed the general focus for such metamaterials to be on energy absorption [16], a high magnitude of elastic strain [7] and vibration isolation [18]. When operating within the confined boundaries, a metamaterial with a bistable unit cell can be restored to its original form by an application of restoration forces. The need for an external force has intrigued the curiosity of metamaterials with a self-restoration ability. Thereby introducing of metastable equilibrium states.

Existing literature related to mechanical systems classified equilibrium states into three main categories. Stable, unstable and neutral equilibrium states [17][12]. However, there exists a forth form of equilibrium state known as a metastable equilibrium state. [1] describes metastability as metastable equilibrium state for which the free energy has a local minimum. For such a state, the system is stable to small fluctuations in the coordinates, but will eventually evolve (possibly after an extremely long time) to a more stable state. Although metastability is commonly observed in nature [14][11], it is rare to see engineered mechanical systems with the properties of metastability. Recently published work by Brinkmeyer [5][6] is one of the few publications on the investigation of metastability in a prestressed beam and hollow semi-spheres. In his work, Brinkmeyer formulated metastability by introducing viscoelastic properties in the prestressed beams and hollow semi-spheres.

With the desire to create new forms of metamaterials, the objective of the masters evolved into classifying various bistable mechanism and transforming bistability of a simple pre-curved beam to metastability, thereby formulating a proof of concept for metamaterials with metastable unit cells. With Brinkmeyers work as inspiration, the metastability is solved by introducing viscoelastic properties in the pre-curved beam.

The structure of this thesis is as follows, The paper on Classifying Bistable systems and Identifying a feasible bistable system that can be redesigned for metastability discusses the literature study related to metastability and the selection of pre-curved beams. Followed by the discussion on solving for metastability in Modelling of Metastable Equilibrium State using PRB Principles. In the end, the report provides a general discussion and conclusion.



# 2

Literature review: Classifying Bistable systems and Identifying a feasible bistable system that can be redesigned for metastability

# Literature review: Classifying Bistable systems and Identifying a feasible bistable system that can be redesigned for metastability

**Krishna Dheeraj Kommuri, Freek Broeren, Just Herder**

Dept. of Precision and Micro Systems Engineering

Dept. of Bio Mechanical Engineering

Delft University of Technology

Delft 2628 CD, The Netherlands

krishnadheeraj.kommuri@gmail.com, f.g.j.broeren@tudelft.nl, J.L.Herder@tudelft.nl

**Milton Aguirre**

Milton Medical B.V.

Amperestraat 214

The Hague 2563 ZZ, The Netherlands

Milton@MiltonMedical.eu

*The literature study presented in this paper focuses on two objectives, objective one is the classification of bistable mechanisms which are the building blocks of some metamaterials and objective two is to identify literature on metastable equilibrium states. The results of both objectives are expected to be used for the formulation of a new building block for metamaterial with metastable equilibrium. The results of such metamaterial can create a self-healing/self-restoring structure. The investigation of the literature study has resulted in the selection of viscoelasticity to realise metastability in a pre-curved beam.*

## 1 Introduction

The metamaterial field of engineering is a fascinating branch with an appetite to fabricate systems with unique properties like negative Poisson's ratio [1], energy absorption [2] and many more. With the advent of such unconventional properties have opened many possibilities in the field of aerospace, medicine, military [1] along with others. Katia Bertoldi's [3] work gives a detailed classification of metamaterials of various forms.

Among the many metamaterials available in the literature, metamaterials with bistable unit cells are the ones that inspired this literature study. Metamaterials with bistable unit cell (basic repeat structures in metamaterials) can exhibit high magnitudes of elastic strain, energy absorption properties [2], returning to initial form [4–7] and vibration damping properties [8]. With the involvement of equilibrium states in metamaterials through bistability, it is given to be intrigued by the idea of introduction of other equilibrium states in metamaterials.

With the possibility of creating new mechanical properties, this literature study has set another foot in the study of various equilibrium states. This curiosity has resulted in an encounter with the Metastable equilibrium state. One of the conventional definitions for metastable states “metastable equilibrium state for which the free energy has a local minimum. For such a state, the system is stable to small fluctuations in the coordinates, but will eventually evolve (possibly after an extremely long time) to a more stable state.” [9] Implying the existence of time vector to the equilibrium state.

This literature study focuses on two objectives; the first objective is to define and identify metastable equilibrium states in mechanical systems, and the latter objective is to classify metamaterials with various bistable unit cells and to select a feasible bistable unit cell that can be redesigned for metastability.

The structure of this literature study is as follows, in section [2] various forms of equilibrium states are defined and section [3.1] presents literature introduction to the metastable equilibrium state. Section [4] gives a brief introduction to metamaterials with bistable unit cells, and section [4.5] gives the classification of various forms of bistable systems. In the end, section [6] offers discussion on metastability and classification of bistable unit cells. Finally, section [7] offers a conclusion on the literature study.

## 2 Equilibrium states

In mechanical systems, a particle is said to be at equilibrium state when the net force acting on the system is zero. Not all equilibrium states are equal. Their potential energy landscape can help distinguish them apart. For the sake of



simplicity, the nature of the equilibrium state can be visualised [figure – potential energy landscape] by a ball rolling on a varying terrain; in this case, the terrain would be the potential energy landscape, and the ball represents the state of the particle.

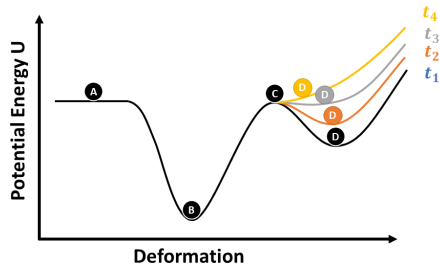


Fig. 1: Different forms of equilibrium states expressed using a ball, A - neutral equilibrium, B - stable equilibrium, C unstable equilibrium and D - metastable equilibrium

Figure [1] is the potential energy (y-axis) representation of a particle over a range of deformation (x-axis).

### 2.1 Neutral equilibrium

From the figure 2, when the particle is at position A, the potential energy for a small band of deformation does not vary. The net energy needed for the particle to move within the band is zero. Study lamps are one of the common appliances with neutral equilibrium nature [10] [11].



This Photo by Unknown Author is licensed under CC BY-SA

Fig. 2: Example for neutral equilibrium, study lamp. A study lamp can remain any orientations (with in the range of the motion) without the need for activation.

### 2.2 Stable equilibrium

From the figure 3, when the particle is at position B, it is considered to be at global minima. Any deviation experienced by the particle when at stable equilibrium will even-

tually bring the particle back to its initial state. The magnitude of energy needed to get the particle out is relatively high compared to any other equilibrium states. A regular pendulum is a conventional system with stable equilibrium properties [10, 11].

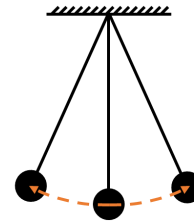


Fig. 3: Example for stable equilibrium, pendulum. Here a pendulum is shown to depict stable equilibrium and any disturbance applied on the pendulum will eventually place the pendulum normal to the ground.

### 2.3 Unstable equilibrium

From the figure 4, when the particle is at position C, it is considered to be at unstable equilibrium. An unstable equilibrium is defined as a local maxima on a potential energy landscape. A typical example of an unstable equilibrium would be an inverted pendulum [10, 11].

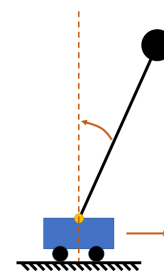


Fig. 4: Example for unstable equilibrium, Inverted pendulum. Here the cart is depicted to balance inverted pendulum by constantly counter the fall of inverted pendulum by moving the cart in the direction of fall.

### 2.4 Metastable equilibrium

So far, from section 2.1 to section 2.3 described equilibrium states independent of time. As stated in the earlier definition, metastability is time-dependent. From the figure

1, When the particle is at point D. It continues to stay D for a short duration before returning to a stable equilibrium. A poppy toy can attain metastability under specific conditions.

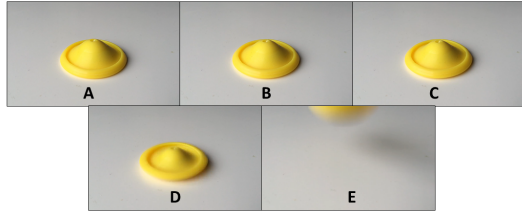


Fig. 5: Example for metastable equilibrium, sequence of images showing different stages of progression from metastable to stable equilibrium.

### 3 Metastability

Section 2 offered intuitive examples for various equilibrium states. Whereas this section offers existing research which is done on metastable equilibrium and also shares various examples for the metastable phenomenon that happens in nature.

#### 3.1 Existing research on metastability

Metastable equilibrium states in mechanical systems is a relatively recent topic. Brinkmeyer's work [12, 13] is the only work available on the topic of metastability, although Brinkmeyer refers to metastability as pseudo bistable behaviour. His work on viscoelastic hallow semi-sphere [13] and viscoelastic pre-stress beam [12] is valuable at identifying the metastable behaviour in the respective geometries. Brinkmeyer was able to quantify the time needed for either of the geometries to return to their original forms when left to recover after deformation. Brinkmeyer's has investigated the influence of geometric parameters, material parameters and manufacturing parameters on metastability.

##### 3.1.1 Nature examples

Although there is not much existing research on metastability in mechanical systems, there are various phenomenon that are governed by metastability. The most observed metastability phenomenon would be seed dispersal [3, 14, 15]. Despite the result of the dispersion of the seeds are irreversible for the pod, the self-activation brought the pod structure from local minima to the global minima. This behaviour can be associated with metastability.

References [11, 16] explicitly stated metastability in biomechanics (in humans) through internal activation of

muscles — work by [17] defined metastability as a local minima which is independent of time. According to Armin Kibele's work metastability is defined in humans as the ability to maintain stability for small perturbations whereas Armin Kibele's work [11] defined metastability as a state that falls in between stable and unstable equilibrium, giving the ability to define running most efficiently.

The following table gives an accumulation of nature-inspired metastability with a brief note

### 4 Metamaterials

The ability to influence the mechanical properties by varying the geometry has created an array of applications for metamaterials. Applications based on negative Poisson's ratio, energy absorption, refractive index and many more. In this section, the influence of bistable unit cell design on mechanical properties is discussed.

The common objective in literature for metamaterials with bistable unit cells is to solve for Energy absorption, Vibration Isolation and Shape reconfiguration. Literature offered various bistable solutions aiming at these problem statements.

#### 4.1 Energy Absorption

Metamaterials with energy-absorbing properties are designed intending to absorb shock and preventing the propagation of shock through the metamaterial. Sicong Shan's work [19] demonstrated the influence of energy absorption by storing the energy within the system through elastic deformation [figure 6]. Making the metamaterial structure restorable to its original form.

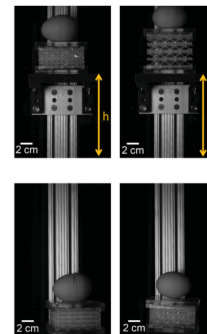


Fig. 6: This figure compares the energy absorbing behaviour of bistable metamaterial by presenting structure ability to protect egg from cracking [19]

#### 4.2 Vibration Isolation

Hang Yang's work [20] has investigated the behaviour of bistable unit cell metamaterials under vibration. Because of buckling based bistability in the unit cells. The resonance frequency has moved to the left. Improving the operating

Reference	Application	Working Principle Followed for Metastability
[11]	Bipedal running	Rapid oscillation of the centre of mass projection from within the support polygon to out of the support polygon.
[17]	Bipedal balancing	Rapid activation and relaxation of muscles to maintain balance.
[16]	Seed dispensing	As time progresses the internal pressure of the pod increases, whereas the roots of the pod (place where pod is attached to the plant) dries and gets brittle. At a point internal pressure exceeds and the root of the pod gives away, causing an explosion of the pod.
[14]	Seed dispensing	As time progresses the inner walls are well hydrated but the other walls get drier. Fibre pattern on the outer wall support curling. When the pod is matured the stiffness difference is high enough for the walls to curl outwards and propelling seeds out.
[18]	Seed dispensing and defence mechanism	Similar mechanism compared to [14]

Table 1: References to nature example for metastable equilibrium

frequency of the metamaterials. These metamaterials were design intended to act as mounting docks for high precision applications.

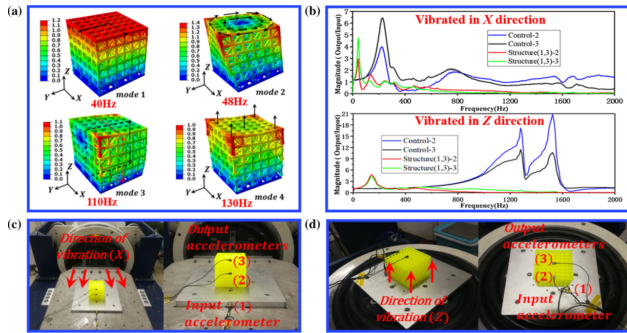


Fig. 7: This figure compares the frequency response between a control structure and a metamaterial 3 dimensional structure [20]

### 4.3 Shape reconfiguration

Because of the high magnitude of elastic strain, bistable metamaterials are often used in space and medical application where real estate is expensive or has additional constraints. Medical stents design [1] and high elastic strain design [2] are some of the many applications of shape re-configuration. Because of the nature of the metamaterials, the deployability of such structures is repetitive and can be achieved with minimum involvement of active components.

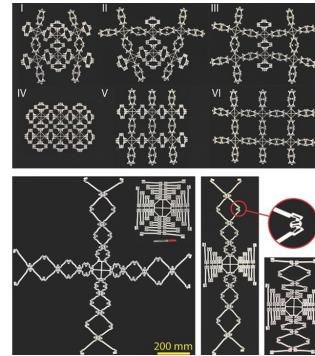


Fig. 8: This figure presents open structures with considerably high dimensions compared to their own close structures [2]

### 4.4 Other mechanical properties

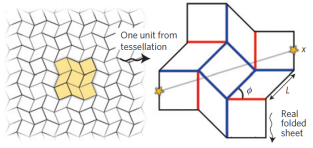
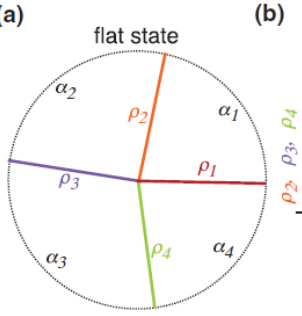
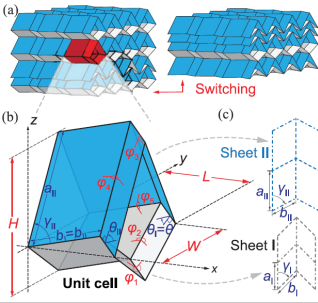
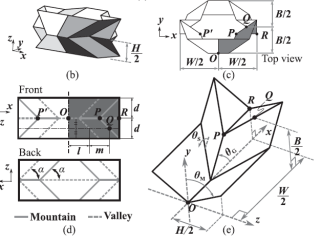
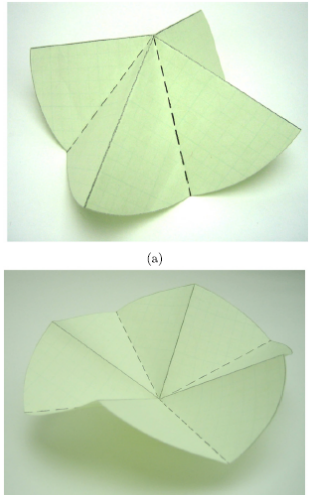
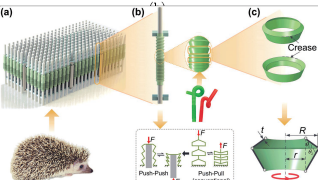
Bistable metamaterials can also influence mechanical properties like Poisson's ratio [21] [20] or the stiffness properties [22]. However, the influence of bistability is only limited to a short bandwidth of deformation. Beyond this bandwidth, the structure acts similar to a conventional geometry with regular mechanical properties.

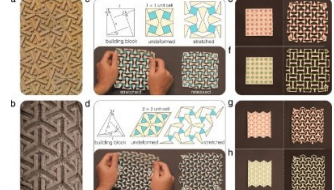
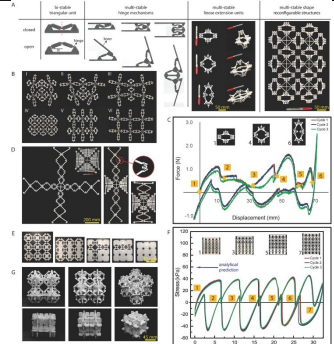
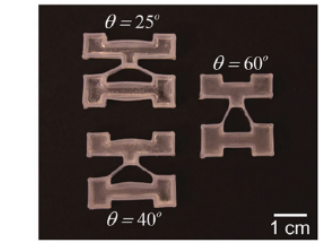
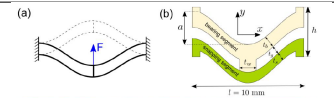
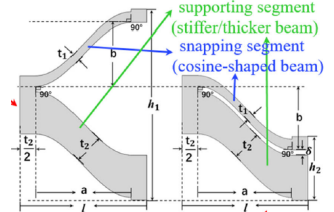
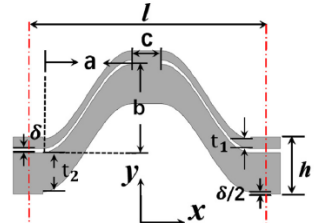
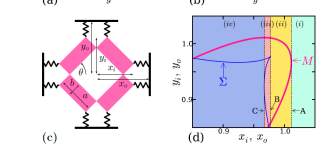
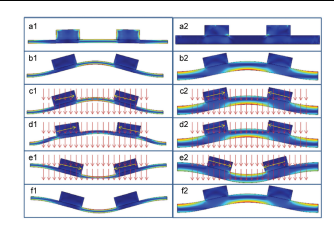
### 4.5 Classifications of Bistable systems

This section lists various forms of bistable unit cell designs which can form a metamaterial. All the bistable unit cells do not follow similar principles to attain metastability, and each structure offers their unique properties. This classification will be later referred in the selection of a simple design. Which will be later researched form metastability.

#### 4.5.1 Relative stiffness Between rigid body and hinge

To attain bistability in the intended origami design [5] is only possible by accounting for the hidden degree of free-

Classification	Source	Unit cell design	Description
Relative stiffness Between rigid body and hinge	[5]		Attains bistability by exploiting the bending stiffness of the facet of the unit cell
Kinematic based instability	[23]	(a) flat state 	The number of stable states in a unit cell are dependent on the arch angle of the facets [a1, a2, a3 and a4].
	[22]	(a) Switching 	Bistability in Miura-ori is due to the kinematic instability. Miura-ori unit cell has unique stiffness behaviour and depends on the applied direction of the deformation.
	[6]	(a) Top view 	Has NPR along one direction and PPR along another direction But Poisson's ratio is not constant
	[24]	(a) 	At both stable states, the valleys and hills remain their orientation.
	[25]	(a) Hedgehog 	Inspired by nature – hedgehog. Similar to a straw with a flexible neck

<p>Relative orientation [Kinematic relation]</p>	<p>[7]</p>		<p>Bistable Auxetic – Poisson’s ratio -1 at max strain. Relative rotation of the hinges causes bi-stability</p>
<p>Buckling based instability</p>	<p>[2]</p>		<p>Shape reconfigurable structure. Auxetic structure Hysteresis force vs displacement response. Returns to initial state after n repetitions.</p>
<p>[19]</p>	<p>[19]</p>		<p>Impact absorption Bistability acts under compression</p>
<p>[21]</p>	<p>[21]</p>		<p>Bistable and acts under tension and zero Poisson’s ratio.</p>
<p>[20]</p>	<p>[20]</p>		<p>Bistable acts under tension Unit cell design and comparison study of parallel and opposite U shape snapping t2/t1 relation to Poisson’s ratio relation is studied.</p>
<p>[26]</p>	<p>[26]</p>		<p>Stiffness along transverse load direction</p>
<p>[27]</p>	<p>[27]</p>		<p>Controlled response of Y axis stress vs strain using X axis strain.</p>
<p>[28]</p>	<p>[28]</p>		<p>Buckling induced instability. Force application for change of state through the interaction of external magnetic field and magnets. Optimise Positioning and orientation of the magnets over the buckling beam.</p>



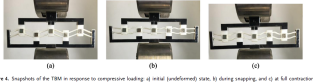
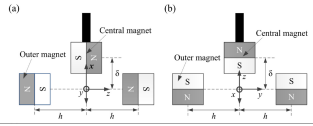
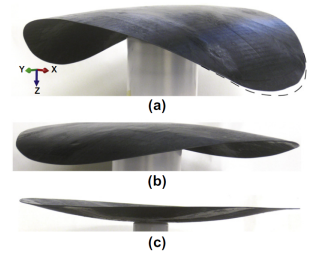
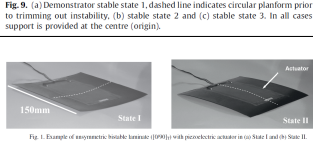
Magnetic actuation and buckling	[29]		Buckling induced instability by tuning the threshold of the instability by introducing magnets
Magnetic actuation	[30]		Investigating instability with different orientation of the magnets Not buckling induced instability
Composites	[31]		Use of curvature and anisotropy to generate different stable states Multistable structure. Controlling the stiffness matrix by the orientation of fibres and layout pattern.
	[32]		Curvature induced instability Controlling the stiffness matrix by the orientation of fibres and layout pattern.

Table 2: Classification of bistable unit cells based on the working principles

dom of the facets (rigid bodies of origami design). Thereby allowing the origami design to achieve bistability. The existence of bistability in such designs is about the stiffness ratio between hinges and the facets of the origami design.

#### 4.5.2 Kinematic based instability

Origami designs dominate this branch of bistability. The relative facet lengths and hinge placements offer bistability. Because of the nature of the unit cell design of Miura-ori [22], the attained stable state is dependent on the direction of applied deformation.

#### 4.5.3 Relative orientation [Kinematic relation]

Bistability in rotating polygon design is associated with the relative rotation between unit cells. Because of the relative rotation, polygon design can attain negative Poisson's ratio.

#### 4.5.4 Buckling based instability

Buckling is generally considered undesirable in classical mechanics because of the drastic change in the stiffness. However, when the desired buckling is in the elastic region and with geometric constrains, buckling based bistability can be achieved [2] [19] [21] [20] [26] [27] [28]. The general focus of the literature with buckling based bistability is energy absorption and shape reconfiguration. The lattice structure of followed in the literature [21] [19] [21] offer zero Poisson's ratio. Metastable design structure discussed in Programmable Mechanical Metamaterials [27] was able to control the magnitude of stress with a control input. In buckling based bistability classification, bistability in the unit cells are

either induced of geometry (pre-curved) [19] [19] [20] [26] and [29] or prestressing of the unit cell [27] and [28]. The significant difference between geometry – buckling based design and prestress – buckling based design is the potential energy landscape of geometry-based buckling is asymmetric while prestress-based buckling is symmetric.

#### 4.5.5 Magnetic actuation and buckling

Work by Tiegang Chen [29] was able to enhance and control the potential energy landscape of the bistable unit cell by introducing magnetic resistance during loading.

#### 4.5.6 Magnetic actuation

Work by Xiaojun Tan [30] is relatively similar to the concept discussed in the [29] except for the bistability is purely because of the magnetic interaction.

#### 4.5.7 Composites

In composite designs, the bistability or some cases multistability is because of the combination of curvature of the structure and stiffness matrix (anisotropy). General applications of composite-based bistability are in aircraft designs.

### 5 Designing for Metastability

The behaviour of metastability as per the figure 1 and the definition presented in the section [1] is due to its ability to change its potential energy landscape. Varying the potential energy can be done by applied deformation or varying the geometry or varying the material properties. Varying the geometry or varying the material properties can be self-

induced, whereas varying applied strain is purely dependent on the environment.

From the literature, Brinkmeyer's work presented in the section [metastability section], attained metastability by utilising viscoelastic material, implying the variation of material properties. Due to limited recourse on the literature front, designing for metastability in the thesis work is ventured through varying material properties. As proof of concept, the objective of the thesis was restated to design a single simple unit cell with metastability. From the available classification of bistable systems, pre-curved beams (buckling based bistability) is selected.

## 6 Observation

The objective of the literature review is two-tier, the first objective is to identify available literature on metastable equilibrium, and objective two is to classify bistable unit cell designs based on the working principle for bistability. Furthermore, combining answers of both objectives to create metamaterial with metastable unit cell.

The literature on metastability in mechanical systems is relatively short when compared to the literature on metamaterials. With the literature as the reference, a simple pre-curved beam with dominant viscoelastic properties is selected to realise a proof of concept for the metastable unit cell.

As stated in the section [5], metastability can also be achieved by varying geometry, and the feasibility of such a concept can be tested with various bistable mechanisms presented in the table [4.5].

## 7 Conclusion

Literature study followed in this thesis has investigated metastable equilibrium state and bistable unit cell designs in metamaterials. This investigation has presented the work of Brinkmeyer on pseudo bistable systems (same as metastability), and classification of bistable mechanisms into seven individual categories. Following the literature review, a simple pre-curved beam with viscoelastic properties is selected as the proof of concept for a metastable unit cell.

## References

- [1] Ren, X., Das, R., Tran, P., Ngo, T. D., and Xie, Y. M., 2018. "Auxetic metamaterials and structures: a review". *Smart Materials and Structures*, **27**(2), jan, p. 23001.
- [2] Haghpanah, B., Salari-Sharif, L., Pourrajab, P., Hopkins, J., and Valdevit, L., 2016. "Multistable Shape-Reconfigurable Architected Materials". *Advanced Materials*, **28**(36), pp. 7915–7920.
- [3] Bertoldi, K., Vitelli, V., Christensen, J., and van Hecke, M., 2017. "Flexible mechanical metamaterials". *Nature Reviews Materials*, **2**, oct, p. 17066.
- [4] Gatt, R., Mizzi, L., Azzopardi, J. I., Azzopardi, K. M., Attard, D., Casha, A., Briffa, J., and Grima, J. N., 2015. "Hierarchical Auxetic Mechanical Metamaterials". *Scientific Reports*, **5**, feb, p. 8395.
- [5] Silverberg, J. L., Na, J.-H., Evans, A. A., Liu, B., Hull, T. C., Santangelo, C., Lang, R. J., Hayward, R. C., and Cohen, I., 2015. "Origami structures with a critical transition to bistability arising from hidden degrees of freedom". *Nature Materials*, **14**, mar, p. 389.
- [6] Yasuda, H., and Yang, J., 2015. "Reentrant Origami-Based Metamaterials with Negative Poisson's Ratio and Bistability". *Phys. Rev. Lett.*, **114**(18), may, p. 185502.
- [7] Rafsanjani, A., and Pasini, D., 2016. "Bistable auxetic mechanical metamaterials inspired by ancient geometric motifs". *Extreme Mechanics Letters*, **9**, pp. 291–296.
- [8] Antoniadis, I. A., Kyriakopoulos, K. J., and Papadopoulos, E. G., 2017. "Hyper-Damping Behavior of Stiff and Stable Oscillators with Embedded Statically Unstable Stiffness Elements". *International Journal of Structural Stability and Dynamics*, **17**(05), p. 1740008.
- [9] , 2010. "Nucleation in Condensed Matter: Applications in Materials and Biology". In *Nucleation in Condensed Matter*, K. F. Kelton and A. L. Greer, eds., Vol. 15 of *Pergamon Materials Series*. Pergamon, p. iii.
- [10] Sygne, J. L., 2008. *Principles of Mechanics*. Milward Press.
- [11] Kibele, A., Granacher, U., Muehlbauer, T., and Behm, D. G., 2015. "Stable, Unstable and Metastable States of Equilibrium: Definitions and Applications to Human Movement". *Journal of sports science & medicine*, **14**(4), nov, pp. 885–887.
- [12] Brinkmeyer, A., Santer, M., Pirrera, A., and Weaver, P. M., 2012. "Pseudo-bistable self-actuated domes for morphing applications". *International Journal of Solids and Structures*, **49**(9), pp. 1077–1087.
- [13] Brinkmeyer, A., Pirrera, A., Santer, M., and Weaver, P. M., 2013. "Pseudo-bistable pre-stressed morphing composite panels". *International Journal of Solids and Structures*, **50**(7), pp. 1033–1043.
- [14] Vaughn, K. C., Bowling, A. J., and Ruel, K. J., 2011. "The mechanism for explosive seed dispersal in *Cardamine hirsuta* (Brassicaceae)". *American Journal of Botany*, **98**(8), pp. 1276–1285.
- [15] Vincent, O., Weißkopf, C., Poppinga, S., Masselter, T., Speck, T., Joyeux, M., Quilliet, C., and Marmottant, P., 2011. "Ultra-fast underwater suction traps". *Proceedings of the Royal Society B: Biological Sciences*, **278**(1720), pp. 2909–2914.
- [16] Morillon, R., Liénard, D., Chrispeels, M. J., and Lassalles, J.-P., 2001. "Rapid Movements of Plants Organs Require Solute-Water Cotransporters or Contractile Proteins". *Plant Physiology*, **127**(3), pp. 720–723.
- [17] Kibele, A., Classen, C., Muehlbauer, T., Granacher, U., and Behm, D. G., 2014. "Metastability in plyometric training on unstable surfaces: a pilot study". *BMC sports science, medicine & rehabilitation*, **6**, jul, p. 30.
- [18] Yano, S., 1997. "Silique burst of *Cardamine scutata* (Cruciferae) as a physical inducible defense against

- seed predatory caterpillars”. *Researches on Population Ecology*, **39**(1), jun, pp. 95–100.
- [19] Shan, S., Kang, S. H., Raney, J. R., Wang, P., Fang, L., Candido, F., Lewis, J. A., and Bertoldi, K., 2015. “Multistable Architected Materials for Trapping Elastic Strain Energy”. *Advanced Materials*, **27**(29), pp. 4296–4301.
- [20] Yang, H., and Ma, L., 2019. “Multi-stable mechanical metamaterials by elastic buckling instability”. *Journal of Materials Science*, **54**(4), feb, pp. 3509–3526.
- [21] Rafsanjani, A., Akbarzadeh, A., and Pasini, D., 2015. “Snapping Mechanical Metamaterials under Tension”. *Advanced Materials*, **27**(39), pp. 5931–5935.
- [22] Sengupta, S., and Li, S., 2018. “Harnessing the anisotropic multistability of stacked-origami mechanical metamaterials for effective modulus programming”. *Journal of Intelligent Material Systems and Structures*, **29**(14), pp. 2933–2945.
- [23] Waitukaitis, S., Menaut, R., Chen, B. G.-g., and van Hecke, M., 2015. “Origami Multistability: From Single Vertices to Metasheets”. *Phys. Rev. Lett.*, **114**(5), feb, p. 55503.
- [24] Hanna, B. H., Lund, J. M., Lang, R. J., Magleby, S. P., and Howell, L. L., 2014. “Waterbomb base: a symmetric single-vertex bistable origami mechanism”. *Smart Materials and Structures*, **23**(9), aug, p. 94009.
- [25] Pan, F., Li, Y., Li, Z., Yang, J., Liu, B., and Chen, Y., 2019. “3D Pixel Mechanical Metamaterials”. *Advanced Materials*, **31**(25), p. 1900548.
- [26] Yang, H., and Ma, L., 2018. “Multi-stable mechanical metamaterials with shape-reconfiguration and zero Poisson’s ratio”. *Materials & Design*, **152**, pp. 181–190.
- [27] Florijn, B., Coulais, C., and van Hecke, M., 2014. “Programmable Mechanical Metamaterials”. *Phys. Rev. Lett.*, **113**(17), oct, p. 175503.
- [28] Crivaro, A., Sheridan, R., Frecker, M., Simpson, T. W., and Lockette, P. V., 2016. “Bistable compliant mechanism using magneto active elastomer actuation”. *Journal of Intelligent Material Systems and Structures*, **27**(15), pp. 2049–2061.
- [29] Chen, T., Zhang, X., Yan, X., Zhang, B., Jiang, J., Huang, D., Qi, M., and Sun, R., 2019. “Harnessing Magnets to Design Tunable Architected Bistable Material”. *Advanced Engineering Materials*, **21**(3), p. 1801255.
- [30] Tan, X., Chen, S., Wang, B., Zhu, S., Wu, L., and Sun, Y., 2019. “Design, fabrication, and characterization of multistable mechanical metamaterials for trapping energy”. *Extreme Mechanics Letters*, **28**, pp. 8–21.
- [31] Coburn, B. H., Pirrera, A., Weaver, P. M., and Vidoli, S., 2013. “Tristability of an orthotropic doubly curved shell”. *Composite Structures*, **96**, pp. 446–454.
- [32] Bowen, C. R., Kim, H. A., and Salo, A. I. T., 2014. “Active Composites based on Bistable Laminates”. *Procedia Engineering*, **75**, pp. 140–144.



# 3

## Modelling of Metastable Equilibrium State using PRB Principles

# Modelling of Metastable Equilibrium State using PRB Principles

**Krishna Dheeraj Kommuri, Freek Broeren, Just Herder**

Dept. of Precision and Micro Systems Engineering

Dept. of Bio Mechanical Engineering

Delft University of Technology

Delft 2628 CD, The Netherlands

krishnadheeraj.kommuri@gmail.com, f.g.j.broeren@tudelft.nl, J.L.Herder@tudelft.nl

**Milton Aguirre**

Milton Medical B.V.

Amperestraat 214

The Hague 2563 ZZ, The Netherlands

Milton@MiltonMedical.eu

*In this paper, viscoelastic pre-curved beams are used for the study of a time-dependent equilibrium state, also referred to as metastable equilibrium. Formulation of an analytical model of the beam is done by combining an equivalent Pseudo Rigid Body (PRB) model of the pre-curved beam (modelling the beam's compliance) with Standard Linear Solid (SLS) model (modelling the beam's viscoelasticity). Experimental, geometrical and material parameters which can influence metastability are identified. An experimental setup is designed based on the observed parameters to validate the analytical model. Metastability was observed in beams with various geometries. However, conclusive validation of the analytical model can not be established because of the considerable deviation between experimental and analytical results. Introduction of anisotropy into the prototypes through 3D printing is expected to be the major contributing factor for the deviation. This deviation demands the need for repeating the investigation using a prototype made of isotropic material.*

## Nomenclature

t Time

$E_r$  Elastic modulus of the spring used in a SLS model for modelling viscoelasticity

$K_r$  Stiffness of the spring with  $E_r$  as the modulus

$E_v$  Viscoelastic modulus used in a SLS model for modelling viscoelasticity

$K_v$  Stiffness of the spring with  $E_v$  as the modulus

$K_{rlx}$  Stiffness of a simple SLS model under quasi static deformation rate

$K_{int}$  Stiffness of a simple SLS model under infinite deformation rate

$K_{rlx}$  Stiffness of a torsional SLS model under quasi static deformation rate

$K_{int}$  Stiffness of a torsional SLS model under infinite deformation rate

$K_{crlx}$  Stiffness of a compression SLS model under quasi static deformation rate

$K_{cint}$  Stiffness of a compression SLS model under infinite deformation rate

$SLS_{tr}$  SLS model representing viscoelasticity in bending

$SLS_c$  SLS model representing viscoelasticity in compression

$E_{r1}$  Rubber modulus obtained from bending test

$E_{v1}$  Viscoelastic modulus obtained from bending test

$E_{r2}$  Rubber modulus obtained from compression test

$E_{v2}$  Viscoelastic modulus obtained from compression test

$\eta$  Viscosity of the dashpot used in SLS model

$\delta_{Trg}$  Target deformation in a stress relaxation test

$\frac{\partial \delta}{\partial t}$  rate of deformation defined in a stress relaxation test

$t_{rlx}$  relaxation time - period during which  $\delta_{Tr}$  deformation is maintained

$t_{rov}$  Recovery time - time needed for the structure to return to its initial state.

T Thickness of the beam

w Width of the beam

a Span of the beam

b Apex height of the beam measured from the base of the beam

L Arc length of the beam

Q Shape factor of the beam

$\Theta$  Angle between rigid body and the x-axis in a PRB model

$\gamma$  Correction factors used in the estimation the pivot positions in a PRB model

$\mathcal{H}_t$  Heaviside function at time t

## 1 Introduction

Equilibrium states are an important aspect in many scientific field . Within the realm of classical mechanics, potential energy and influence of perturbations are some of the methods followed in the classification of equilibrium states. Stable equilibrium, unstable equilibrium and neutral equilibrium [1] [2] are the most common classifications defined in classical mechanics. Despite the broader definitions when time is considered; stable, unstable and neutral equilibrium do not form the universal set for equilibrium states. This void could be filled with the introduction of a metastable equilibrium state.

A body is said to be in metastable equilibrium if the attained stability in the system is confined to a brief period after which it returns to its initial form without any external influence. Although systems with metastable equilibria are rare in engineered mechanical systems, they are common in nature, chemical science and physics. The seed dispersion mechanism of Ecballium elaterium also commonly known as squirting cucumber plant [3], the decay of chemical bonds or isomers [4] are some of the many examples that fit the definition of metastability.



Fig. 1: Popper toy with metastable equilibrium properties

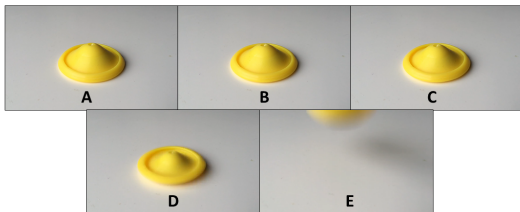


Fig. 2: Different phases of the popper toy in transition from a metastable equilibrium state

One of the most relatable examples and the inspiration

behind this paper for metastable equilibrium state is a popper toy figure 1. It is a hollow half sphere, made of viscoelastic material. Figure 2 shows a sequence of images of deformed popper toy in the metastable equilibrium state.

A. Brinkmeyer's work [5] was one of the first to study metastable equilibria under the name pseudo bistable systems. A. Brinkmeyer's work focused on attaining metastability using viscoelastic behaviour of silicon rubber in prestressed beams. Prony series modelling was followed to capture the viscoelastic behaviour of the silicon rubber. A. Brinkmeyer's work also investigated the influence of geometry, manufacturing, stiffness of the beam and magnitude of pre-stress on metastability.

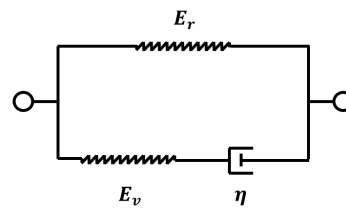


Fig. 3: SLS model representation of viscoelastic materials,  $E_r$  and  $E_v$  are the moduli of the springs and  $\eta$  is the viscosity of the dashpot

This paper investigates metastability in pre-curved beams which are manufactured by 3D printing [for more information on manufacturing refer to the appendix A] with Thermoplastic polyurethane (TPU)[procured from rigid.ink] as the raw material. These pre-curved beams are modelled analytically by combining a Pseudo Rigid body (PRB) model [6] [7] [8] [9] with a Standard Linear Solid (SLS) [figure 3] [10] representation for capturing deformation and viscoelastic behaviour of the beams.

The structure of the paper is as follows, section 2 gives a short introduction on viscoelasticity followed by a discussion on modelling of viscoelasticity using SLS model. In section 3 analytical model describing the force deformation characteristics of a pre-curved beam is derived. Followed by discussion on the conditions for metastability in the section 4. In section 5 analytical model to quantify metastability is derived. Section 6 through 9 offers experimental setup, results and discussion on the results and finally conclusion.

## 2 Viscoelasticity

Viscoelasticity is a material property where a specimen under constant deformation(force) continues to relax(yield) as time progresses. The behaviour of viscoelasticity is attributed to the rearrangement of the lattice structure and loss

of internal energy in the form of heat from within the structure [11].

Literature offers various methods for modelling viscoelasticity. Because of its simplicity the Standard Linear Solid (SLS) model is followed in this paper. An SLS model is made of two springs and a dashpot. Where Spring  $[E_r]$  represents the rubber modulus of the material and spring  $[E_v]$  represents the viscoelastic modulus of the material. The viscosity of the material is represented by a dashpot of viscosity  $[\eta]$ . By using Laplace transformation [10], the force deformation transfer function of an SLS model can be written as,

$$\frac{F(s)}{X(s)} = K_r + \frac{s \cdot K_v}{s + \frac{K_v}{\eta}} \quad (1)$$

Where  $K_r$  is the stiffness calculated with rubber modulus  $E_r$  and  $K_v$  is the stiffness calculated with viscoelastic modulus  $E_v$ . Because of viscoelasticity, the effective stiffness of an SLS model is dependent on the magnitude of deformation and rate of deformation. Under extreme conditions like instantaneous or quasi-static deformation rates the effective stiffness of an SLS model are  $(K_r + K_v) \frac{N}{m^2}$  and  $K_r \frac{N}{m^2}$  respectively.

### 3 Analytical Modelling of pre-curved beam

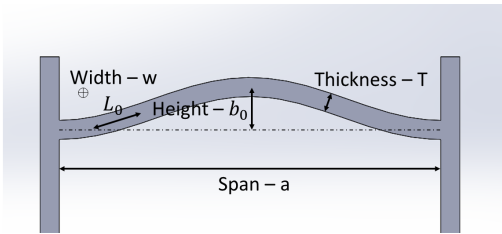
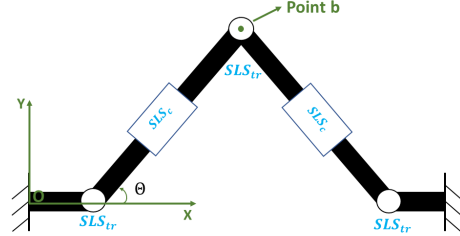


Fig. 4: Pre-curved beam with geometric parameters,  $a$  - span of the beam,  $T$  - Thickness of the beam,  $b_0$  - apex height of the beam and  $w$  - width of the beam

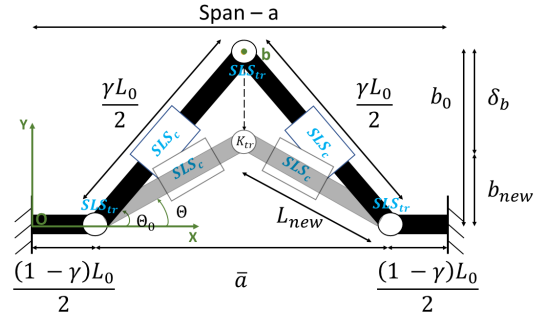
As stated in the introduction, metastability is investigated in a pre-curved beam [figure 4]. In this section, we will be discussing the formulation of the analytical model by integrating an equivalent PRB model of the pre-curved beam with an SLS model springs. The results of the analytical model can help identify geometric and experimental conditions for metastability.

In PRB modelling, springs and rigid bodies are used to represent a compliant body. The building of such models can be done in more than one way, which can introduce redundancies to the model and complicate the analytical solution.

Such redundancies were curbed by observing the deformation shape and following the literature work by LL Howell [7] [6] and literature on pre-curved beams [9] [8]; this resulted in the PRB model shown in the figure 5a [for more details refer to the appendix C].



(a) PRB model with three torsional SLS model springs of stiffness  $SLS_{tr}$  and two compression SLS model springs of stiffness  $SLS_c$ .  $\theta$  as the independent variable and position  $b$  is the point of application of external force



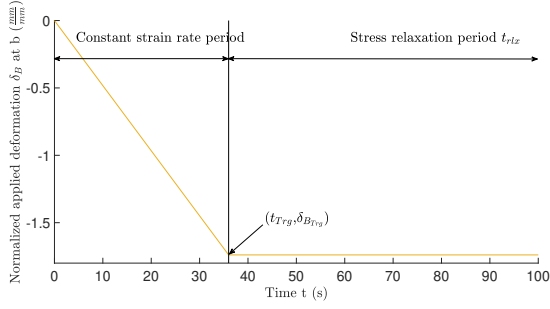
(b) Parametric representation of PRB model followed in deriving the force deformation characteristics of the beam.

Fig. 5: PRB model representation of pre-curved beam

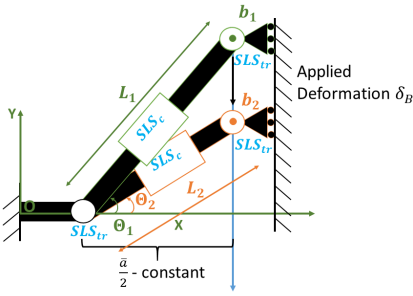
Figure 5b shows the nomenclature followed in building the analytical model of the pre-curved beam and in accounting for viscoelasticity of the material, the springs in the PRB model are formulated using SLS model. Within the scope of the study, the applied deformation at the point  $b$  on the beam is constrained to follow the behaviour shown in the figure 6a.

Since the pre-curved beam is expected to follow mode 1 deformation and the mode 2 deformation is constrained, the resulted trajectory of the point  $b$  is expected to follow straight line parallel to the  $y$  axis [trajectory of the point  $b$  is along the line  $b_1b_2$  - figure 6b]. The resultant deformations at the torsional SLS model  $SLS_{tr}$  and the compression SLS model  $SLS_c$  for the applied deformation [figure 6a] will be perceived as shown in the figures 7 and 8.

Equation 2 gives analytical representation of the deformation at the torsional SLS ( $SLS_{tr}$ ) model as expressed in the figure 7



(a) Applied deformation by an external probe at point b on the beam



(b) Nature of deformation of PRB model influenced by the geometric constraint

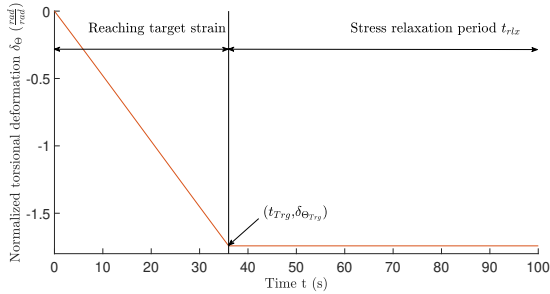


Fig. 7: Deformation of torsional springs by the influence of an applied deformation at point b.

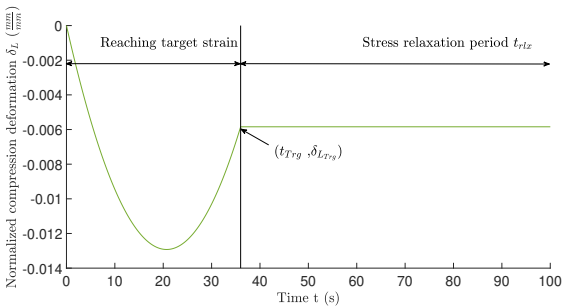


Fig. 8: Deformation of compression springs by the influence of an applied deformation at point b.

$$\delta_{\Theta} = \frac{\partial \delta_{\Theta}}{\partial t} t \cdot (1 - \mathcal{H}_{t_{Trg}}) + \Theta_{Trg} \cdot \mathcal{H}_{t_{Trg}} \quad (2)$$

where  $\frac{\partial \delta_{\Theta}}{\partial t}$  is the deformation rate at  $\Theta$ ,  $\Theta_{Trg}$  is the target deformation and  $\mathcal{H}_{t_{Trg}}$  is a Heaviside function at time  $t = t_{Trg}$  and  $\delta_{\Theta}$  is the instantaneous measured deformation of  $\Theta$ . Equation 3 gives the analytical representation of the deformation at the compression SLS model as expressed in the figure 8

$$\delta_L = \left( \frac{\partial^2 \delta_L}{\partial t^2} t^2 + \frac{\partial \delta_L}{\partial t} \right) \cdot (1 - \mathcal{H}_{t_{Trg}}) + L_{Trg} \cdot \mathcal{H}_{t_{Trg}} \quad (3)$$

where  $\frac{\partial^2 \delta_L}{\partial t^2}$  are  $\frac{\partial \delta_L}{\partial t}$  the acceleration and deformation rate at  $L$ ,  $L_{Trg}$  is the target deformation and  $\mathcal{H}_{t_{Trg}}$  is a Heaviside function at time  $t = t_{Trg}$  and  $\delta_L$  is the instantaneous measured deformation of  $L$ . Frequency domain representation of equation 2 and equation 3 is formulated by applying Laplace transformation

$$\delta_{\Theta}(s) = \mathcal{L}(\delta_{\Theta}) \quad (4)$$

$$\delta_L(s) = \mathcal{L}(\delta_L) \quad (5)$$

The resultant reaction torque for the deformation in equation 4 is calculated by rewriting the stiffness and viscosity coefficients in equation 1 to match to that of bending behaviour of beam.

$$T(s) = \left( K_{Tr} + \frac{s \cdot K_{VTr}}{s + \frac{K_{VTr}}{\eta_{Tr}}} \right) \cdot \delta_{\Theta}(s) \quad (6)$$

where  $K_{Tr}$  and  $K_{VTr}$  are the elastic and viscoelastic torsional stiffness and  $\eta_{Tr}$  is the torsional viscosity. Similarly, the resultant reaction force for the deformation given in equation 5 is also calculated by rewriting the stiffness and viscosity coefficients in equation 1 to match the compression behaviour of the beam.

$$F(s) = \left( K_{rc} + \frac{s \cdot K_{Vc}}{s + \frac{K_{Vc}}{\eta_c}} \right) \cdot \delta_L(s) \quad (7)$$

where  $K_{rc}$  and  $K_{Vc}$  are the elastic and viscoelastic compression stiffness and  $\eta_c$  is the compression viscosity. The time-domain representation of equation 6 and equation 7 are given by applying an inverse Laplace transformation

$$T(t) = \mathcal{L}^{-1}(T(s)) \quad (8)$$

$$F(t) = \mathcal{L}^{-1}(F(s)) \quad (9)$$

With the help of equation 8 and equation 9, the net reaction force at point b offered by the torsional SLS model springs and compression SLS model springs can be analytically expressed as equation 10:

$$F_{Net} = 2 * \sin(\Theta) \cdot F(t) + \frac{8 \cos^2(\Theta)}{\bar{a}} \cdot T(t) \quad (10)$$

#### 4 Conditions for Metastability in Pre-Curved Beams

This section presents experimental, geometric and material conditions which will have to meet the requirements to attain metastable equilibrium.

##### 4.1 Experimental Conditions

Within the scope of this paper, metastability in a pre-curved beam is tested by following stress relaxation method. In an ideal stress relaxation method, the pre-curved beam is deformed instantly to a target deformation and maintained. During this constant deformation period also referred to as relaxation period ( $t_{rlx}$ ), the internal stressed developed in the viscoelastic material are plotted. Figure 9 shows an ideal input conditions of such a stress relaxation test.

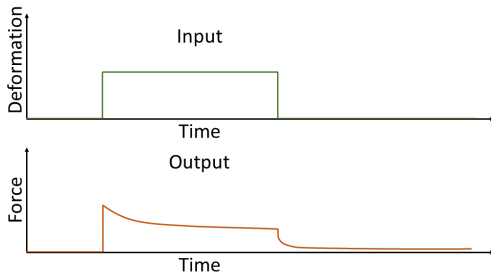


Fig. 9: Stress Relaxation Test - Deformation as input and stress as output.

However, in a practical stress relaxation test, the input and output conditions are similar to figure 10. Based on the figure 10, deformation rate  $\frac{\partial \delta}{\partial t}$ , target deformation  $\delta_{Trg}$  and the relaxation time  $t_{rlx}$  are considered as experimental parameters. For an ideal test condition the peak measured force (stress) is much higher when compared to a practical case.

To achieve metastability in a pre-curved beam, the applied deformation  $\delta_b$ , shown in the figure 6a should be at least a factor of  $\sim 0.7$  of the initial apex height  $b_0$  and a significant relaxation time [ $t_{rlx}$ ](measured using analytical model).

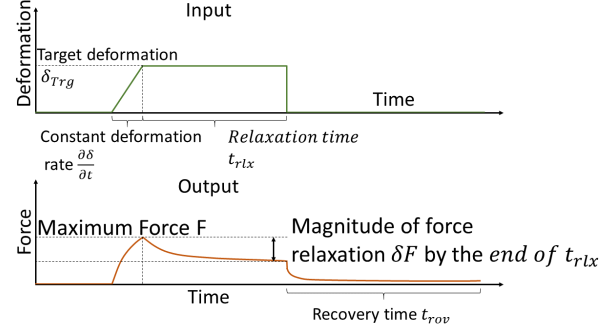


Fig. 10: Stress Relaxation experimental - with deformation rate  $\frac{\partial \delta}{\partial t}$ , target deformation  $\delta_{Trg}$  and relaxation time  $t_{rlx}$  as input parameters. Maximum attained force F, Force relaxation  $\delta F$  and recovery time  $t_{rov}$  are the resultant output characteristic.

##### 4.2 Geometric Parameters

From the figure 4 the thickness - T, span - a, undeformed height of apex -  $b_0$ , width - w and shape factor - Q, (which is a ratio of thickness to the undeformed height of the apex of the beam -  $\frac{b_0}{T}$ ) are the geometric parameters. Work by Hussein Hussein [8] offers insights into the static force deformation characteristics of the pre-curved beam in terms of shape factor Q. According to the Hussein Hussein's work, for shape factor  $Q < 2.314$ , a single pre-curved beam will act as a mono-stable system and for  $Q > 2.314$  pre-curved beams act as a bi-stable system. On observation, it has been noticed that a bistable beam does not get into metastable equilibrium. therefore, pre-curved beams with shape factors  $Q < 2.314$  are preferred for the study of metastability. For the sake of convince thickness T and span a are set to 3mm and 60mm respectively. Along with testing for a proof of concept, this paper also looks at the influence of shape factor Q on metastability.

##### 4.3 Material Parameters

In this section, the influence of material properties on metastability is discussed.

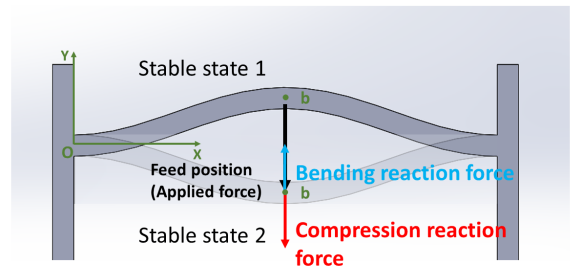


Fig. 11: Nature of bending and compression forces at point b near possible stable state 2

In a conventional pre-curved beam where the viscoelasticity of the material is considered insignificant, the possibility of bistability is a combined factor of bending and compression forces. In the figure 11 we can see the resultant reaction forces generated by bending and compression forces at the point b. With the introduction of viscoelasticity, the magnitude of bending and compression reaction forces are dependent on deformation duration and deformation rate resulting in relaxation of force as time progresses. A temporary stability can be obtained if the order of relaxation of bending force is greater than the order of compression force. Based on this principle, A. Brinkmeyer [5] was able to develop the following relation between bending and compression stiffness of the material.

$$\left(1 - \frac{K_{t_{rlx}}}{K_{t_{ist}}}\right) > \left(1 - \frac{K_{c_{rlx}}}{K_{c_{ist}}}\right) \quad (11)$$

where  $K_{t_{rlx}} \frac{N^*s}{m^2}$  is the relaxed stiffness and  $K_{t_{ist}} \frac{N^*s}{m^2}$  is the instantaneous stiffness of torsion springs. Whereas,  $K_{c_{rlx}} \frac{N}{m^2}$  is the relaxed stiffness and  $K_{c_{ist}} \frac{N}{m^2}$  is the instantaneous stiffness of compression springs. For a simple SLS model [fig. 3] the effective instantaneous stiffness is  $(K_r + K_v) \frac{N}{m^2}$  and relaxed stiffness is  $K_r \frac{N}{m^2}$ .

Evaluating the condition [equation 11] depends on the viscoelastic material properties. [Refer to the appendix D to learn more about procedures involved in the evaluation of material properties].

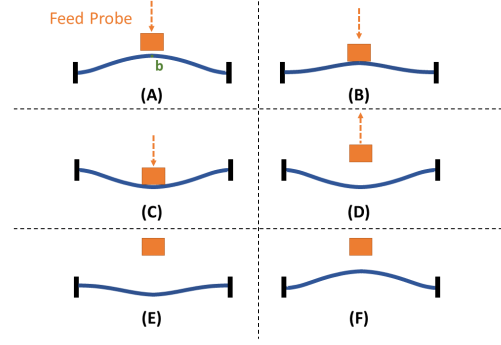
## 5 Recovery Time Estimation

So far, the paper has introduced the analytical model and parameters that influence metastability. This section defines the measure of metastability and ways to quantify it.

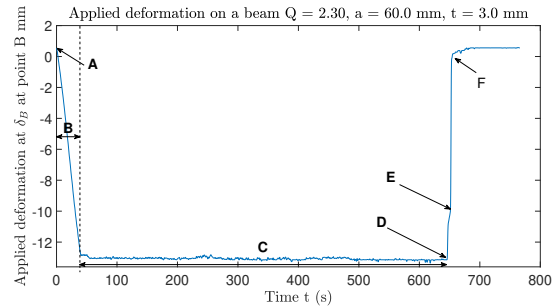
The magnitude of metastability in a pre-curved beam is quantified by the recovery time needed for the beam to return to its original form following deformation. If the observed recovery time is not zero, then the beam is considered to be in metastable equilibrium.

Figure 12 indicates the deformation of the beam with respect to the position of point b over time. Work by A. Brinkmeyer [5] explained the force deformation profile of a pre-stressed beam during recovery. According to A. Brinkmeyer's work, at the end of relaxation time (following the retraction of feed probe) beam is expected to deform to D instantly and the measure of time needed for the beam to travel the path D to E is considered as the recovery time. At point E, the bending force dominates [figure 11] and restores the beam instantly to its original form.

To analytically translate the above-described work to a PRB model, one would need an understanding of the complex interaction between all springs and optimisation of the internal energy, which would introduce a high order complexity to the problem statement. The following assumption was made to simplify the behaviour, "The rate of stiffness re-



(a) Progression of the beam deformation over time during a stress relaxation test



(b) Position of point b overtime of a beam during stress relaxation test, with the undeformed initial position as reference  $\delta_b = 0$ . Beam geometry specifications  $Q = 2.3$ ,  $T = 3mm$  and  $a = 60mm$

Fig. 12: Multiple stages of beam deformations during stress relaxation. A - Initial undeformed for of the beam, B - Constant applied deformation rate,  $\frac{\partial \delta_b}{\partial t} = 20 \frac{mm}{min}$ , C - Stress relaxation period for  $t_{rlx} = 600$  seconds. D - Quick retract of the feed probe, E - Snap back position and F - fully restored beam

covery of SLS model spring is not influenced by the presence of any other SLS springs defined within the PRB model."

By following the assumption, the effective recovery time of the beam is estimated by quantifying the time needed for the torsional SLS spring to travel the path D to E [figure 12]. [Since torsional springs contribute to the restoration of the beam]

$$\delta = \delta_{Tr} e^{-\frac{K_r}{\eta} \left(1 - \frac{K_r}{K_v}\right)^{-1} t} \quad (12)$$

With the help of the assumption, the recovery rate of torsional SLS spring is derived resulting in the equation 12 [12][refer to the appendix B for detailed derivation]

## 6 Experimental Setup

Section 3 and section 4 have introduced an analytical model and conditions for metastability. Formulation of these models is based on various assumptions and linearization of the pre-curved beam. Experimental validation is needed in order to verify the assumptions. This section introduces the



test bench design that was followed to validate and recreate metastability.

As a side note, the viscoelastic material properties of TPU material are needed to validate the analytical model and metastable condition. Appendix D gives a detailed description of the experimental design for quantifying material properties.

## 6.1 Test bench design

As stated earlier, the scope of this paper is to test for metastability in pre-curved beams by performing a stress relaxation test. From the figure 10 we know the input parameter for stress relaxation is deformation  $[\delta_b]$  and the resistance to the deformation is defined as the output. Zwick Z005 tensile test bench was selected for testing metastability on the pre-curved beams as the input and output parameters defining the stress relaxation are within the operational range of the tensile test bench.

Although the tensile test bench can accommodate the desired deformation rate and also maintain the deformation, it cannot retract fast, as fast retraction is needed to facilitate the beam to recover uninterrupted [frame D in figure 12a]. The fast retraction is achieved by using a solenoid as a feed probe. Figure 13 shows the assembly of the solenoid setup.

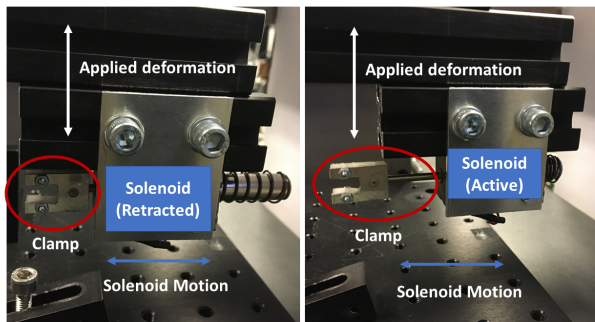


Fig. 13: Right - Retracted solenoid, Left - Activated solenoid. Solenoid is set to move parallel to the ground, whereas the applied deformation  $\delta_b$  moves normal to the ground.

### 6.1.1 Clamp design

A pre-curved beam under load can go into mode-2 deformation because of error in probe position or non-uniform beam thickness (because of manufacturing) or because of the inherent unconstrained rotational degree of freedom of the beam. By using a planar contact for load application the mode-2 deformation can be mitigated. clamp design shown in figure 14 is used during the experimental procedure. The Poly Carbonate clamp is sandwiched stainless steel to improve the normal stiffness of the clamp.

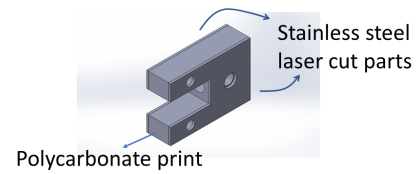


Fig. 14: Poly-carbonate clamp design reinforced with stainless steel to improve the stiffness the clamp.

### 6.1.2 Prototype setup

Analytical models are solved with zero initial conditions, which means zeros force at zero deformation. Such zero initial conditions are emulated by taking measures to avoid introduction of stress in the specimen while mounting and maintaining same geometries under before the start of the test. figure 15 is a picture in which prototype is mounted and prestress are mitigated by using a spacer (red circle).

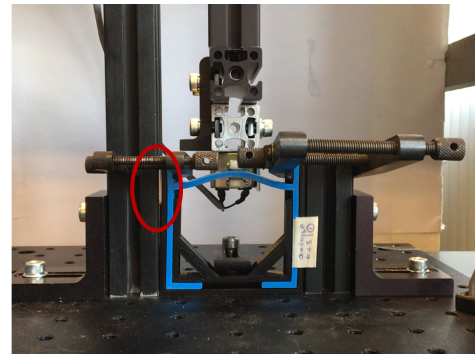


Fig. 15: Placing a spacer (in the red circle) between beam and the setup to mitigate pre-tensioning of the beam. Existence of pre-tension is verified by measuring span a of the beam

## 7 Results

### 7.1 Material Test Results

Viscoelastic properties of TPU are tested for bending, compression and tensile forces. Table [1] to table [5] states all the experimental conditions and critical dimensions of the test specimens used in material testing, refer appendix D for detailed information on procedures followed for estimation of material properties.



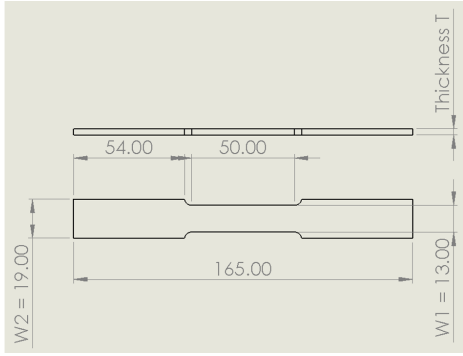


Fig. 16: Specimen dimensions used in testing for material properties of TPU under tensile load. Specimens with thickness 3 mm and 5 mm are tested.

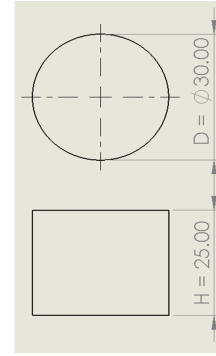


Fig. 17: Specimen dimensions used in testing for material properties of TPU under compression load.

### 7.1.1 Tensile Test

Specimen Dimension	Experiment parameters	Test results
T = $2.93 \pm 0.0167$ mm	$\delta = 5$ mm	$E_r = 3.5e+07$ N/m <sup>2</sup>
W1 = $13.17 \pm 0.0096$ mm	$\frac{\partial \delta}{\partial t} = 10$ mm/min	$E_v = 6.6e+06$ N/m <sup>2</sup>
W2 = $19.13 \pm 0.0167$ mm	$t_{rlx} = 20$ min	$\eta = 5.5e+05$ Ns/m

Table 1: Experimental results of tensile test of 3 mm thick dogbone specimen

### 7.1.2 Compression Test

Specimen Dimension	Experiment parameters	Test results
Diameter = $29.68 \pm 0.1424$ mm	$\delta = 0.5$ mm	$E_r = 1.03e+07$ N/m <sup>2</sup>
Height = $25.04 \pm 0.0385$ mm	$\frac{\partial \delta}{\partial t} = 1.2$ mm/min	$E_v = 1.74e+06$ N/m <sup>2</sup>
	$t_{rlx} = 20$ min	$\eta = 1.30e+07$ Ns/m

Table 3: Experimental results of compression test

Specimen Dimension	Experiment parameters	Test results
T = $5.05 \pm 0.0193$ mm	$\delta = 5$ mm	$E_r = 3.17e+07$ N/m <sup>2</sup>
W1 = $13.17 \pm 0.0255$ mm	$\frac{\partial \delta}{\partial t} = 10$ mm/min	$E_v = 5.7e+06$ N/m <sup>2</sup>
W2 = $19.10 \pm 0.0048$ mm	$t_{rlx} = 20$ min	$\eta = 9.1e+05$ Ns/m

Table 2: Experimental results of tensile test of 5 mm thick dogbone specimen

### 7.1.3 Bending Test

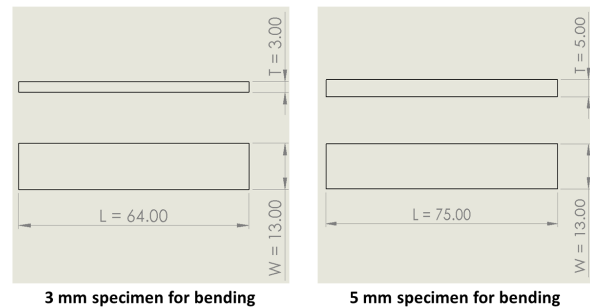


Fig. 18: Specimen dimensions used in testing for material properties of TPU under bending deformation. Specimens with thickness 3 mm and 5 mm are tested.

Specimen Dimension	Experiment parameters	Test results
$T = 2.93 \pm 0.0334$ mm	$\delta = 5.5$ mm	$E_r = 1.27e+8$ N/rad · m <sup>2</sup>
$W = 13.07 \pm 0.0167$ mm	$\frac{\partial \delta}{\partial t} = 11$ mm/min	$E_v = 2.45e+07$ N/rad · m <sup>2</sup>
	$t_{rlx} = 20$ min	$\eta = 3.96$ Nm · s/rad

Table 4: Experimental results of bending test of 3 mm thick specimen

Specimen Dimension	Experiment parameters	Test results
$T = 5.02 \pm 0.0441$ mm	$\delta = 7$ mm	$E_r = 8.72e+07$ N/rad · m <sup>2</sup>
$W = 13.12 \pm 0.0585$ mm	$\frac{\partial \delta}{\partial t} = 14$ mm/min	$E_v = 1.61e+07$ N/rad · m <sup>2</sup>
	$t_{rlx} = 20$ min	$\eta = 10.64$ Nm · s/rad

Table 5: Experimental results of bending test of 5 mm thick specimen

## 7.2 Prototype Results

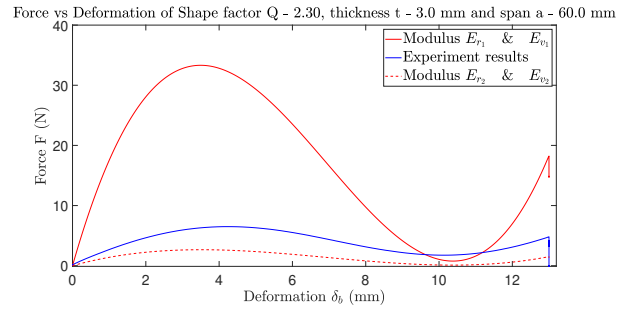
Table 6 gives the experimental parameters followed for investigation of metastability by performing stress relaxation test on the prototypes. Section 7.2.1, section 7.2.2 and section 7 present the results which are analytically estimated and experimentally measured by testing pre-curved beams of dimensions shape factor  $Q$  2.3 and 2.25, with thickness  $T$  3mm and span  $a$  60mm. Each geometry is repeated by 3 samples (shape factor  $Q$  2.3 - 3 samples and shape factor  $Q$  2.25 - 3 samples).

Experiment parameters	Magnitude
deformation $\delta_b$	13 mm
deformation rate $\frac{\partial \delta_b}{\partial t}$	20 mm/min
Relaxation time $t_{rlx}$	10 min

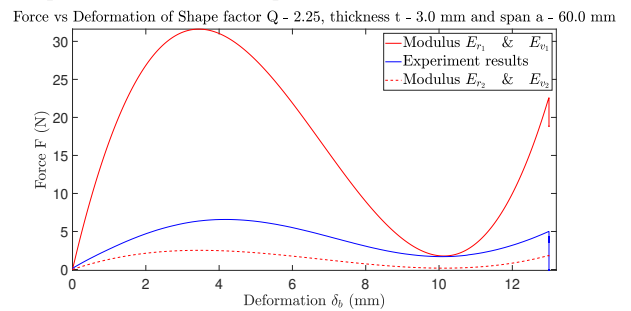
Table 6: Experimental parameters followed in prototype testing

### 7.2.1 Force Deformation Results

This section presents the force deformation plots generated by comparing analytical model and experimental testing of pre-curved beams of dimensions  $Q = 2.3$  and  $Q = 2.25$ ,  $T = 3$ mm and  $a = 60$ mm.  $E_{r1}$  and  $E_{v1}$  are the derived Young's modulus from 3 mm bending test [table 4] and where  $E_{r2}$  and  $E_{v2}$  are the derived Young's modulus from compression test [table 3].



(a) Force deformation behaviour of pre-curved beam with shape factor  $Q = 2.3$ . Analytical results (red plots) are compared with the experimental results (blue plot).

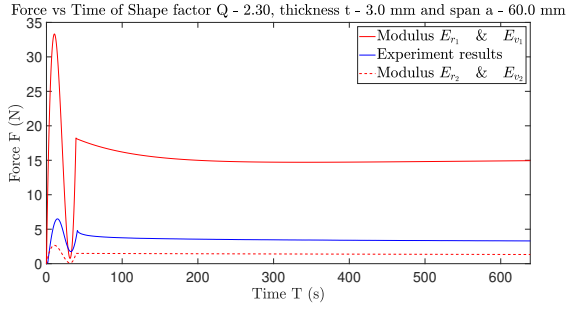


(b) Force deformation behaviour of pre-curved beam with shape factor  $Q = 2.25$ . Analytical results (red plots) are compared with the experimental results (blue plot).

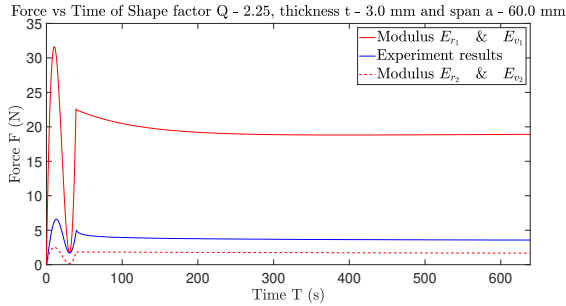
Fig. 19: Comparing the force deformation behaviour results between analytical and experimental test.  $E_{r1}$  and  $E_{v1}$  are the Young's modulus derived from bending test of 3 mm specimens and  $E_{r2}$  and  $E_{v2}$  are the Young's modulus derived from compression testing.

### 7.2.2 Force-Time Results

This section presents the stress relaxation plots generated using analytical model and prototype testing of pre-curved beams of dimensions  $Q = 2.3$  and  $Q = 2.25$ ,  $T = 3$ mm and  $a = 60$ mm.  $E_{r1}$  and  $E_{v1}$  are the derived Young's modulus from 3 mm bending test [table 4] and where  $E_{r2}$  and  $E_{v2}$  are the derived Young's modulus from compression test [table 3].



(a) Force vs time behaviour of pre-curved beam with shape factor  $Q = 2.3$ . Analytical results (red plots) are compared with the experimental results (blue plot).



(b) Force vs time behaviour of pre-curved beam with shape factor  $Q = 2.25$ . Analytical results (red plots) are compared with the experimental results (blue plot)

Fig. 20: Comparing the force vs time behaviour results between analytical and experimental test.  $E_{r1}$  and  $E_{v1}$  are the Young's modulus derived from bending test of 3 mm specimens and  $E_{r2}$  and  $E_{v2}$  are the Young's modulus derived from compression testing.

### 7.2.3 Recovery Time

Table 7 presents the recovery time  $t_{rov}$  measured during the test of pre-curved beams of shape factors  $Q = 2.3$  and  $Q = 2.25$ . The measured recovery time is compared with the analytically estimated recovery time.

Shape Factor	Analytical Recovery Time ( $E_{r1}$ and $E_{v1}$ )	Analytical Recovery Time ( $E_{r2}$ and $E_{v2}$ )	Experimental Recovery Time (mean)
$Q = 2.3$	8.3 s	93 s	4.97 s
$Q = 2.25$	5.1 s	52 s	3.07 s

Table 7: Analytically and experimentally estimated recovery time.  $E_{r1}$  and  $E_{v1}$  are the Young's modulus derived from bending test of 3 mm specimens and  $E_{r2}$  and  $E_{v2}$  are the Young's modulus derived from compression testing.

## 8 Discussion

Results of analytical model predicted metastability in with shape factor  $Q = 2.3$  and  $Q = 2.25$  for thickness  $T = 3mm$  and  $T = 5mm$  and span  $a = 60mm$  and  $a = 100mm$ . Due to inconsistency on the test conditions metastability was only observed in beams with shape factor  $Q = 2.3$  and  $Q = 2.25$  thickness  $T = 3mm$  and span  $a = 60mm$ . Since the material test resulted in different bending and compression Young's modulus the analytical model is tested twice, once with with bending modulus  $E_{r1}$  and  $E_{v1}$  and ones with  $E_{r2}$  and  $E_{v2}$ . On comparing the experimental results with two sets of data (figure 19a and figure 19b) we can say the experimental results fall inside the extreme of the analytical model. The following section will present with the possible reasoning from the deviations observed.

### 8.1 Manufacturing

For the manufacturing of the prototypes, fused deposition modelling (FDM) 3D printing was followed. Despite maintaining consistency between the specimens by following the same settings and print orientation, anisotropy properties are still observed. The possible sources for anisotropy are the orientation of material deposition, variation in the extruder temperature, variation of void volume percentage between specimens. Although 3D printing offered flexibility in design variation, it has introduced a higher degree of anisotropy. As an alternative, silicon rubber casting or water jut cutting of silicon sheets can be considered. Although silicon casting can introduce higher degree of deviation compared to water jet cutting of silicon sheets. Because maintaining consistent resin mixture, curing temperature and poring can be challenging. For future research water jet cut silicon prototypes are recommended because water jet cutting does not introduce heat during fabrication and viscoelastic material properties are sensitive to heat.

### 8.2 Prototype design and experimental setup

The predicted trend of the force deformation behaviour of the beams is in agreement with the experimental observations except at the local minima. Based on the analytical model, the expected magnitude of force at the local minima is close to zero N as opposed to the experimental results where the magnitude of the force is higher. A possible explanation for the deviation could be the deformation of the support structures during loading [figure 21]. An alternative prototype design similar to figure 22 could solve this problem.

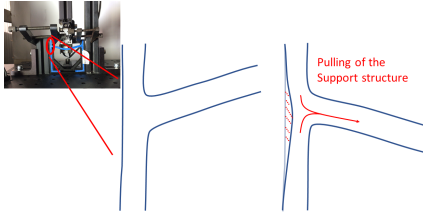


Fig. 21: Deformation at the intersection of the beam base and support structure. Magnitude of the deformation varies as the applied deformation  $\delta_b$  is progressed from 0 to  $\delta_{bTrg}$

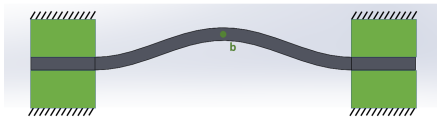


Fig. 22: Alternative beam design to mitigate support structure deformation

On analysing the recorded video of the deformation, the beam appears to show varying degree of mode 2 [figure 23] deformation which could also explain the observed higher magnitude force at the local minima. A sensible solution to constraint mode 2 deformation would be to maintain lower tolerance on the beam thickness, consistent positioning of the clamp and constraining the rotation of the beam.

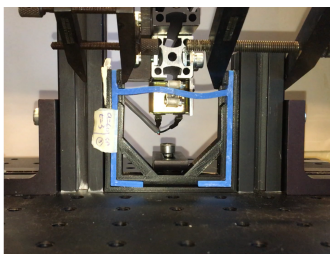


Fig. 23: Appearance of mode 2 deformation of the beam during the transition when applied deformation  $\delta_b$  progresses from 0 to  $\delta_{bTrg}$

### 8.3 Recovery time assumption

In the section 5, an assumption on the interaction between SLS model springs was stated to solve for the beam's recovery time. On comparing the estimates with the experimental observations, we can say the analytical model has overestimated the recovery time. This deviation could be a

reference to the anisotropy of the material or the assumption [section 5] not holding the ground. The ambiguity behind the cause could be solved by repeating the tests on an isotropic pre-curved beam and comparing the experimental results with the analytical results.

## 9 Conclusion

Based on the results presented in the section 7, we can prove the possibility of metastability in pre-curved beams. The observed difference in the recovery time results between the beams with Q 2.3 and Q 2.25 also emphasise the influence of the geometry. However, the lack of agreement between analytical and experimental results can not validate the model. This discrepancy in the results can be associated with the anisotropic behaviour of the prototype, unconstrained mode 2 deformations of the beam and influence of beam and clamp interaction during tests. By considering the recommendation offered in the section 8 like, prototyping using water jet cutting of silicon sheets for minimising anisotropy, revised prototype and clamp design to constraint mode 2 deformation could alleviate the discrepancy and bring forth the metastable properties of the pre-curved beam.

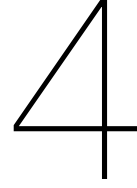
The introduction of metastability has opened new avenues with the ability to operate independently without the need for any additional instruments. Such devices can have numerous applications in medicine, aerospace, automotive and more. In the given period, this paper was able to present with material estimation, analytical modelling of the beam along with the viscoelastic properties. The paper was able to present metastability in an experimental environment and quantify recovery time.

## References

- [1] Syngé, J. L., 2011. *Principles Of Mechanics*. Read Books Limited.
- [2] Kibele, A., Granacher, U., Muehlbauer, T., and Behm, D. G., 2015. "Stable, Unstable and Metastable States of Equilibrium: Definitions and Applications to Human Movement". *Journal of sports science & medicine*, **14**(4), nov, pp. 885–887.
- [3] Forterre, Y., Marmottant, P., Quilliet, C., and NOBLIN, X., 2016. "Physics of rapid movements in plants". *Europhysics News*, **47**, pp. 27–30.
- [4] Prague Summer School on Mathematical Statistical Physics (5th : 2006 Prague, C. R., Biskup, M., and Kotecky, R. T. A. T. T., 2009. *Methods of contemporary mathematical statistical physics LK* - <https://tudelft.on.worldcat.org/oclc/458574884>.
- [5] Brinkmeyer, A., Pirrera, A., Santer, M., and Weaver, P. M., 2013. "Pseudo-bistable pre-stressed morphing composite panels". *International Journal of Solids and Structures*, **50**(7), pp. 1033–1043.
- [6] Lusk, C., 2013. *Using Pseudo-Rigid Body Models*. John Wiley & Sons, Ltd, ch. 5, pp. 55–76.
- [7] Jensen, B., 2013. *Modeling of Large Deflection Members*. John Wiley & Sons, Ltd, ch. 4, pp. 45–54.

- [8] Hussein, H., Le Moal, P., Bourbon, G., Haddab, Y., and Lutz, P., 2015. “Modeling and stress analysis of a pre-shaped curved beam: Influence of high modes of buckling”. *International Journal of Applied Mechanics*, **07**(04), p. 1550055.
- [9] Jin Qiu, Lang, J. H., and Slocum, A. H., 2004. “A curved-beam bistable mechanism”. *Journal of Microelectromechanical Systems*, **13**(2), apr, pp. 137–146.
- [10] Roylance, D., 2001. ENGINEERING VISCOELASTICITY. Tech. rep., Massachusetts Institute of Technology.
- [11] NPTEL, 2012. Introduction to vibration control.
- [12] Ge, Q., Yu, K., Ding, Y., and Jerry Qi, H., 2012. “Prediction of temperature-dependent free recovery behaviors of amorphous shape memory polymers”. *Soft Matter*, **8**(43), pp. 11098–11105.





## Discussion

This section of the report explains the derived results and offers suggestions that can aid in future research for the validation of metastable equilibrium.

Based on the results shared in the paper Modelling of Metastable Equilibrium State using PRB Principles, it can be stated that metastable equilibrium is possible in the pre-curved beam, but the deviation between analytical results and experimental observations can not prove or disprove the designed analytical model. For the sake of quick fabrication, the author decided to follow the 3D printing of TPU filament; which could be the reason behind the introduction of anisotropy in the prototypes. Since the derived analytical model is based on isotropic material, it is advisable to reformulate the analytical model to account for anisotropy or prototyping with an isotropic material (silicon casting or waterjet cutting of silicon sheets

The observed anisotropy could also be associated with the procedure followed in the estimation of material properties of TPU material. The possibility of error can lie in the fabrication of the specimen or the experimental procedure. To mitigate any discrepancy generating from estimating material properties, the author would like to suggest the use of well-established materials and protocols.

The experimental procedure followed in the validation of metastability involved hand calibration of the test bench, this could have introduced inconsistency between tests, the introduction of prestresses and error in positioning of the clamp. Errors in the positioning of the clamp had caused observable mode 2 deformation in the beams. To avoid repetition of errors in future tests, the procedure followed in the fixture of the prototype, design of the prototype and the design of the clamp has to be revised.

Results of the recovery time derived from the analytical model are not in agreement with the measured recovery time. The cause for the overestimated results can either be associated with anisotropy or the stated assumption in deriving the analytical model is false. Validation of the analytical model can only be done by repeating the tests using isotropic material and following the suggestions stated earlier for the experimental procedure.





# 5

## Conclusion

This thesis has developed an analytical model to predict metastable behaviour in a viscoelastic pre-curved beam. Although experimental results prove metastability in pre-curved beams with shape factor Q 2.3 and Q 2.25, the results derived from the analytical model are not in agreement with the experimental results. It is the same case for force behaviour and recovery time estimation. The reasons associated with the deviation of the results could be attributed to various factors ranging from manufacturing to testing.

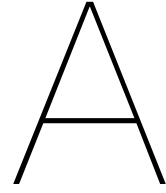
The mean measured recovery time between shape factor Q 2.3 and shape factor Q 2.25 show a difference of  $\approx 2$  seconds. This difference in recovery time between different shape factors can be associated with the influence of geometric parameter Q on metastability. However, because of the deviation in the derived recovery time, the analytical model could neither prove nor disprove the experimental results. The validity of the analytical model can only be proved by repeating all the tests with a prototype made of isotropic material and by following the standard test procedures.

Metastability in a pre-curved beam is dependent on various parameters but limited by the scope of building a proof of concept this thesis has only investigated the influence of shape factor Q. Influence of other parameters could result in the higher difference in the relaxation time. Along with the task of repeating the tests for validating the analytical model and shape factor Q, the future work should also investigate the influence of other parameters on metastability in pre-curved beams.

The assumption made for the formulation of recovery time remains unproven, and as future research, the readers are encouraged to investigate for the recovery time by estimating the energy landscape of the beam at every time step till the beam completely recovers.

The concept of fusing metamaterials with metastability is an intriguing proposition. The work presented in this thesis has opened up various opportunities for future research. In the duration of the thesis, an analytical model of a viscoelastic pre-curved beam was created, metastability in a pre-curved beam was achieved, and the influence of geometric parameters on metastability was proved. The potential magnitude of application that can spur from the topic of the metamaterial can span medicine, aerospace, automotive and many more.





## Appendix: 3D printer settings

In the scope of this project, all the prototypes needed for material testing and the validation of metastability are manufactured using an FDM 3D printer. The following table offers a detailed description of the printer settings.

Parameter	Dimension
Print volume	220x220x250 $mm^3$
Nozzle diameter	0.4 mm
Layer height	0.15 mm
Initial layer thickness	0.06 mm
Initial layer line width	130 %
Shell thickness 1.2 mm Bottom/Top layer thickness	0.75 mm
Fill Density	80 %
Print	Speed 10 mm/s
Bottom layer speed	7 mm/s
Bed temperature	70°C
Nozzle temperature	210°C
Filament diameter	1.75 mm
Filament Flow Percent (%)	102 %

Table A.1: 3D printer settings followed in the manufacturing of the material testing specimens and prototypes



# B

## Appendix: SLS Model Behaviour

### B.1. SLS Transfer Function Modelling

An SLS model is made of three elements, two springs and a dashpot system. Following section details the steps involved in deriving the transfer function of the SLS model

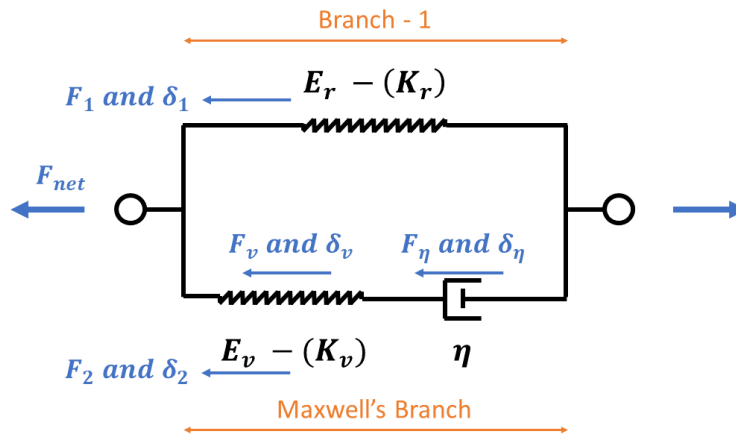


Figure B.1: Forces and deformations experienced by different elements in an SLS model

Maxwells part of the SLS model: Since  $K_v$  and  $\eta$  are in parallel, the forces experienced by  $K_v$  and  $\eta$  are the same, and the total deformation experienced by Maxwells branch is the summation of deformation experienced by  $K_v$  and  $\eta$

$$F_2 = F_v = F_\eta \quad (B.1)$$

$$\delta = \delta_v + \delta_\eta \quad (B.2)$$

$$F_v = k_v \cdot \delta_v \quad (B.3)$$

$$F_\eta = \eta \cdot \dot{\delta}_\eta \quad (B.4)$$

applying a time derivative to the equation B.2 and using the equations B.1,B.3 and B.4

$$\dot{\delta}_2 = \dot{\delta}_v + \dot{\delta}_\eta \quad (\text{B.5})$$

$$\dot{\delta}_2 = \frac{\dot{F}_v}{k_v} + \frac{F_\eta}{\eta} \quad (\text{B.6})$$

$$\dot{\delta}_2 = \frac{\dot{F}_2}{k_v} + \frac{F_2}{\eta} \quad (\text{B.7})$$

Applying Laplace transformation to the equation B.7

$$S \cdot \delta_2(s) = \frac{s \cdot F_2(s)}{K_v} + \frac{F_2(s)}{\eta} \quad (\text{B.8})$$

$$F_2(s) = \frac{s \cdot K_2}{s + \frac{K_2}{\eta}} \cdot \delta_2(s) \quad (\text{B.9})$$

Including branch 1 with the Maxwells branch, Since branch 1 and the Maxwell's branch are in parallel the following conditions apply

$$F_{net} = F_1 + F_2 \quad (\text{B.10})$$

$$\delta_1 = \delta_2 \quad (\text{B.11})$$

$$F_1 = K_r \cdot \delta_1 \quad (\text{B.12})$$

$$F_{net} = K_r \cdot \delta_2 + F_2 \quad (\text{B.13})$$

Introducing equation B.9 in equation B.13 and applying Laplace transformation.

$$F_{net}(s) = K_r \cdot \delta_r(s) + \frac{s \cdot K_2}{s + \frac{K_2}{\eta}} \cdot \delta_2(s) \quad (\text{B.14})$$

$$\delta_r(s) = \delta_2(s) = \delta(s) \quad (\text{B.15})$$

Because branch 1 and Maxwell's branch are in parallel, results in the equation B.15, and combining equation B.15 with B.14 results in the transfer function of a SLS model spring

$$\frac{F_{net}(s)}{\delta(s)} = K_r + \frac{s \cdot K_2}{s + \frac{K_2}{\eta}} \quad (\text{B.16})$$

## B.2. Force response for Constant deformation

Formulating the ideal conditions describing a stress relaxation test on a simple SLS model [figure B.1]. rate of deformation  $\frac{\partial \delta}{\partial t}$  is considered instantaneous, Piece-wise representation of applied deformation in a ideal stress relaxation test is as following

$$\delta(t) = \delta_{Trg} \cdot \mathcal{H}_0 \quad (\text{B.17})$$

here  $\delta_{Trg}$  is the applied constant deformation and  $\mathcal{H}_0$  is the Heaviside function at time  $t = 0$ . Applying Laplace transformation to the equation B.17.

$$\delta(s) = \frac{\delta_{Trg}}{s} \quad (\text{B.18})$$

Substituting equation B.18 in equation B.16 and applying inverse laplace.

$$F(s) = (K_1 + K_2 \cdot e^{-\frac{K_2 t}{\eta}}) \cdot \delta_{Trg} \quad (\text{B.19})$$

### B.3. Recovery Time estimation

Estimating the recovery time of a simple SLS model [figure B.1]. Conditions for the estimating recovery time is no external force acting on the SLS model,  $F_{net} = 0$ , at this point  $K_r$  and  $K_v$  are opposing on another.

$$F_{net} = K_r \delta_1 + K_v \delta_v = 0 \quad (\text{B.20})$$

$$\delta_v = -\frac{K_r \delta_1}{K_v} \quad (\text{B.21})$$

Internal forces in Maxwell's branch of SLS model are as equation B.22

$$F_\eta = F_v \quad (\text{B.22})$$

$$\eta \dot{\delta}_\eta = K_v \delta_v \quad (\text{B.23})$$

$$\dot{\delta}_\eta = \frac{K_v \delta_v}{\eta} \quad (\text{B.24})$$

Writing  $\delta_\eta$  in terms of  $\delta_1$  by substituting equation B.21 in equation B.24

$$\dot{\delta}_\eta = -\frac{K_r \delta_1}{\eta} \quad (\text{B.25})$$

Relating deformation in the Maxwell's branch to deformation in branch 1

$$\delta_1 = \delta_2 \quad (\text{B.26})$$

$$\delta_1 = \delta_v + \delta_\eta \quad (\text{B.27})$$

$$\dot{\delta}_1 = \dot{\delta}_v + \dot{\delta}_\eta \quad (\text{B.28})$$

Writing equation B.28 in terms of  $\delta_1$  by substituting equation B.25 and equation B.21 and rearranging terms

$$\left(1 + \frac{K_r}{K_v}\right) \dot{\delta}_1 = -\frac{K_v}{\eta} \delta_1 \quad (\text{B.29})$$

Applying integration to the equation B.29 with an assumption deformation at the start of recovery time as  $\delta_{1_0}$  will result in the equation B.30

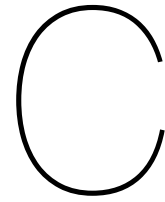
$$\delta_1(t) = \delta_{1_0} e^{-\frac{K_v}{\eta} \left(1 + \frac{K_r}{K_v}\right)^{-1} t} \quad (\text{B.30})$$

rarranging the equation B.30 will result in B.31

$$t = \log\left(\frac{\delta_{1_0}}{\delta_1(t)}\right) \frac{\eta}{K_v} \left(1 + \frac{K_r}{K_v}\right) \quad (\text{B.31})$$

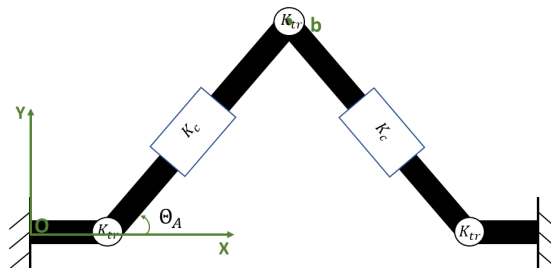




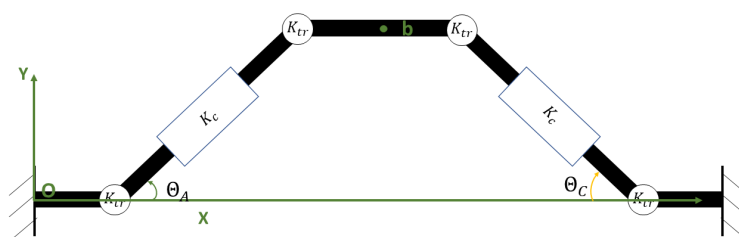


# Appendix: PRB Model selection

## C.1. Appendix: PRB model design



(a) PRB model A with three torsional springs of stiffness  $K_{tr}$  and two compression springs of stiffness  $K_c$ .  $\theta_A$  as the independent variable and position B is the point of application of external force



(b) PRB model B with four torsional springs of stiffness  $K_{tr}$  and two compression springs of stiffness  $K_c$ .  $\theta_A$  and  $\theta_C$  are the two independent variables and position B is the point of application of external force

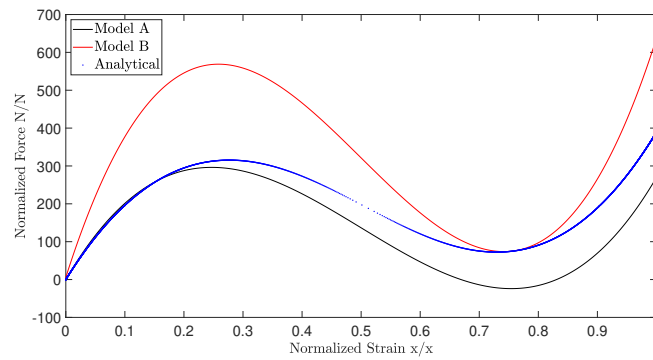
Figure C.1: PRB models

Formulating the best PRB model of the beam needs knowledge in optimal positioning of the pivot points, introducing correction factors for the stiffness to compensate for errors in positioning of the pivot point and path/form of the deformation, the required information was sourced from the work of Larry L. Howell[9][13] which resulted in two PRB models.

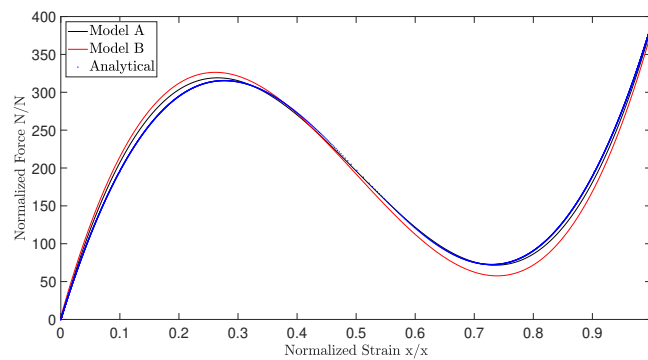
PRB model A [fig. C.1a] is designed using three torsional springs to represent bending stiffness and two compression springs to represent compression stiffness of the pre-curved beam. The symmetric deformation (straight path of travel for point b along the negative y-axis) of the PRB model A is fairly similar to the deformation form of the pre-curved beam with constrained mode 2.

Whereas PRB model B [fig. C.1b] is designed using four torsional springs to represent bending stiffness and two compression springs to represent compression stiffness of the pre-curved beam. The symmetric deformation (straight path of travel for point b along the negative y-axis) of the PRB model B mimics better deformation form of the pre-curved beam with constrained mode 2.

Handbook of Compliant Mechanisms [8] was used to estimate the position of the pivot points and correction factors for the stiffness of the springs. The force deformation characteristics of the PRB models based on the literature correction factors [8] resulted in figure [C.1]. The PRB models did not agree with the analytical result [figure C.2a]. The deviation between the PRB and analytical model is solved by updating the correction factors for both torsional and compression springs by referring to the analytical model. The results of new correction factors resulted in figure [C.2b].



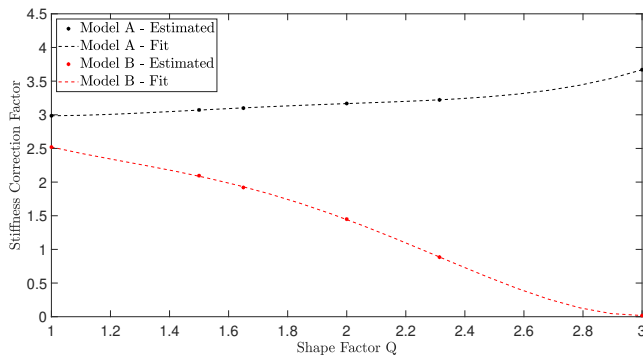
(a) Black plot is the behaviour of the closest PRB model A of the beam with correction factors derived from the literature. Red curve is the behaviour of the closest PRM model B of the beam with correction factors derived from Handbook of Compliant Mechanisms [8]. Blue curve is the behaviour of the beam derived based on the work of [10]



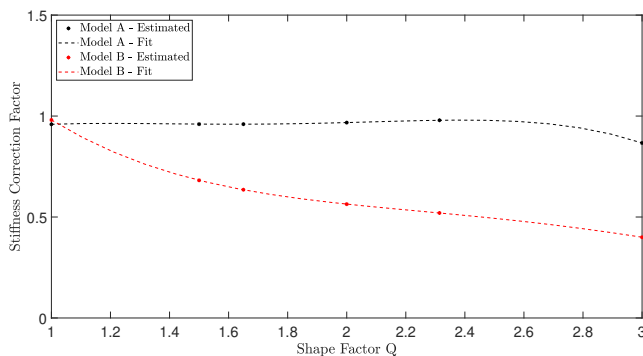
(b) Black plot is the behaviour of the closest PRB model A of the beam with updated correction factors derived from the literature. Red curve is the behaviour of the closest PRM model B of the beam with updated correction factors derived from Handbook of Compliant Mechanisms [8]. Blue curve is the behaviour of the beam derived based on the work of [10]

Figure C.2: Normalised force deformation characteristics of a pre-curved beam with shape factor  $Q = 2$ , span  $a = 100mm$  and thickness  $t = 3mm$ .

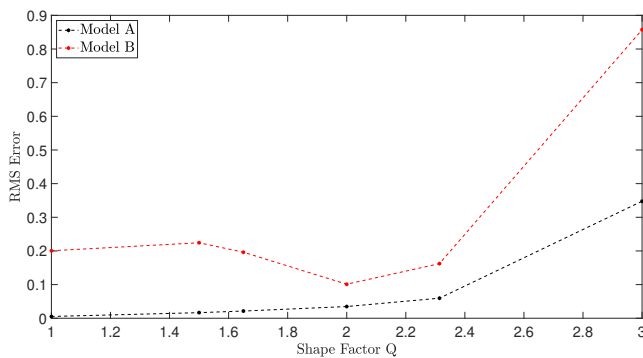
From the figure C.3 we can tell PRB model A happens to have consistent correction factors for the desired shape factors  $Q$  and relatively low RMS error when compared to PRB model B., For this reason, PRB model A is selected to be used for further analytical development.



(a) Updated correction factors of bending springs in both PRB models for various shape factors Q between 1 and 3. \* represent the estimated correction factors and -- are the polynomial fit based on the estimated correction factors written as function of shape factor Q.



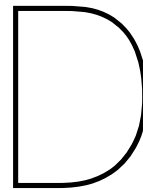
(b) Updated correction factors of compression springs in both PRB models for various shape factors Q between 1 and 3. \* represent the estimated correction factors and -- are the polynomial fit based on the estimated correction factors written as function of shape factor Q.



(c) Estimated RMS error of both models using updated correction factors when compared to the analytical [10]

Figure C.3: Re-evaluation of correction factors





## Appendix: Material Test

This appendix offers test standards followed in identifying the material properties of TPU under bending, tensile and compression deformations.

### D.1. Bending Test

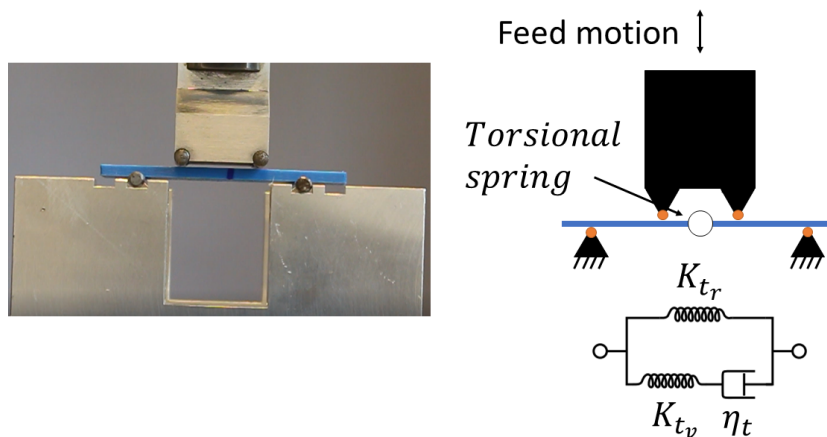


Figure D.1: On the left: Testing setup for a 4 point bending test of a 3mm thick beam. On the right: An equivalent PRB model of the specimen.

For bending test ASTM standard (D6272 - 17)[3] document is referred. Based on the reference geometries shown in the figure D.2 are selected for testing. The maximum allowable mid-span deflection was calculated based on the definition mentioned in the reference document[3]. To accommodate the easy of bending 5mm and 3mm thick beams followed different support span dimensions.

PRB model form referred in the figure D.1 was expected to emulate the closest bending behaviour. This model was used to fit the experimental data to estimate the bending parameters. The applied deformation was considered to be instantaneous, and the resultant torque behaviour followed the equation D.1

$$T(t) = K_{t_r} + K_{t_v} e^{-\left(\frac{K_{t_v} t}{\eta_t}\right)} \quad (D.1)$$

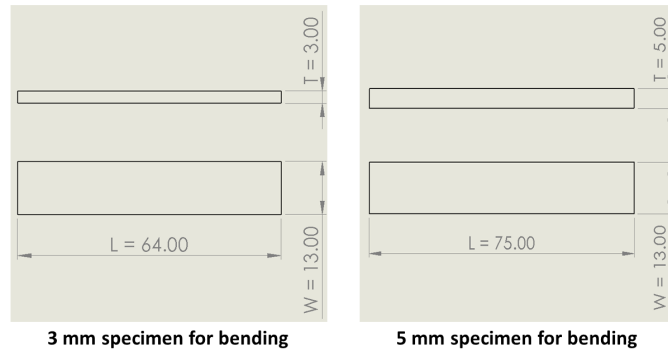


Figure D.2: Specimen dimensions used in testing for material properties of TPU under bending deformation. Specimens with thickness 3 mm and 5 mm are tested.

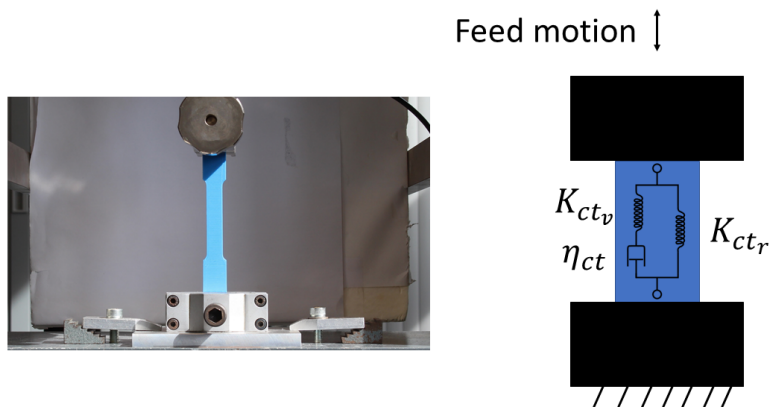


Figure D.3: On the left: Testing setup for tensile test of 3mm thick dogbone. On the right: An equivalent PRB model of the specimen.

## D.2. Tensile Test

For this procedure type I [2][figure D.4] dogbone structure was used to perform stress relaxation under tensile stress. Planar dimensions of the 3mm and 5mm thick specimens were kept constant.

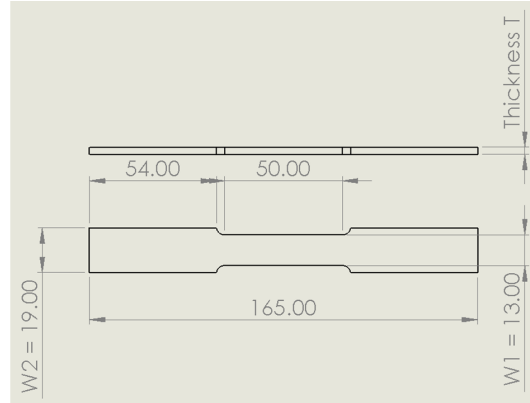


Figure D.4: Specimen dimensions used in testing for material properties of TPU under tensile load. Specimens with thickness 3 mm and 5 mm are tested.

PRB model from the figure D.3 was followed to estimate the material properties under tension. The applied strain was considered to be instantaneous, and the resultant force behaviour followed the equation D.2

$$F(t) = K_{ct_r} + K_{ct_v} e^{-\left(\frac{K_{ct_v} t}{\eta_{ct}}\right)} \quad (D.2)$$

## D.3. Compression Test

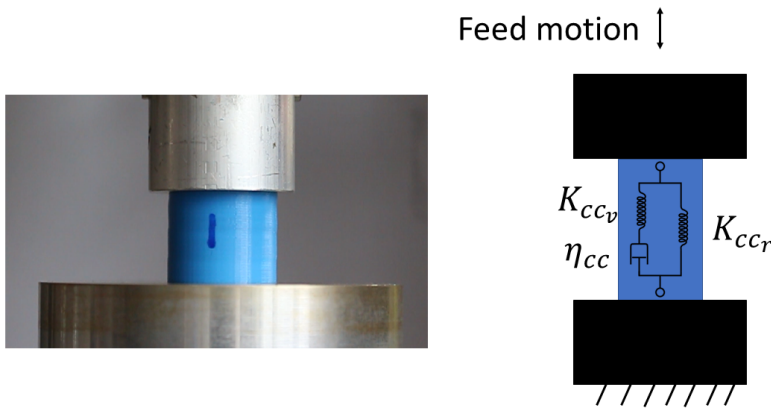


Figure D.5: On the left: Testing setup for a compression test. On the right: An equivalent PRB model of the specimen.

For compression ASTM standard E9[4] document is referred. According to the documentation, there are two acceptable specimen geometries, cylinder or cubes. The ideal case, cubes would have been the best pick as the specimen dimensions are driven based on the thickness. However, because of the small dimensions and introduction of the uneven surface during manufacturing, cylindrical geometry was considered as the best choice [figure D.6].

Specimen with the diameter of 30mm and height of 25mm was picked from the available aspect ratios.

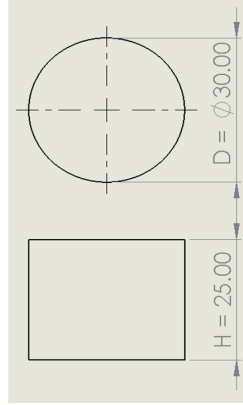
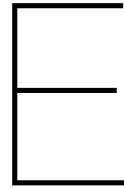


Figure D.6: Specimen dimensions used in testing for material properties of TPU under compression load.

To estimate the material parameters when under compression, a similar PRB model from the D.2 was followed [fig. D.5]. Similar to previously mentioned procedures, the applied strain was considered to be instantaneous and resultant force was expected to follow the equation D.3.

$$F(t) = K_{ccr} + K_{ccv} e^{-\left(\frac{K_{ccv} t}{\eta_{cc}}\right)} \quad (\text{D.3})$$





## Appendix: Matlab Script

```
1 % This LaTeX was auto-generated from MATLAB code.
2 % To make changes, update the MATLAB code and republish this document.
3
4
5
6 %\subsection*{Contents}
7
8 \begin{itemize}
9 \setlength{\itemsep}{-1ex}
10 \item Declaration
11 \item Mechanical properties
12 \item Deriving Force – Deformation behaviour
13 \item PLots
14 \item Recovery time estimation =
15 \end{itemize}
16
17 % Analytical formulation of force – deformation behaviour of viscoelastic
18 % pre-curved beams – To study metastability
19
20 % Krishna Dheeraj Kommuri
21 % 4734173
22 % BioMechanical Design Engineering
23
24 clc
25 clear
26 close all
27
28
29
30 \subsection*{Declaration}
31
32
33 Para.P_Vel          = 20/60000; % Deformation rate in m/s
34
35 Para.RDur           = 10*60;    % Relaxation rate
36
37 SP.Q                = 2.3;      % Q = b0/t, where b0 = initial apex height
38 SP.t                = 3/1000;   % t = thickness of the beam
39 SP.a                = 60/1000;  % a = span of the beam
40 SP.gamma            = 0.8517;   % gamma = referenced from literature
```

```

41 SP.b0      = SP.Q*SP.t;% b0 = initial apex height of the beam
42 SP.W      = 8/1000; % w = width of the beam
43 SP.Ar     = SP.W*SP.t;% Ar = Cross section area of the beam
44 SP.I      = SP.W*SP.t^3/12; % I = area moment of inertia (Normal
45           % to thickness)
46
47 Para.ConstStrain = round(1.9*SP.Q*SP.t*1000)/1000; % delta_Trg
48
49 Xv        = 0:SP.a/10:SP.a;
50 Yv        = (SP.b0/2)*(1 - cos(2*pi*Xv/SP.a));
51
52 SP.L0     = 0; % L0 = arc length of the beam
53
54 for ii = 1:length(Xv) - 1
55     SP.L0 = SP.L0 + sqrt((Xv(ii)-Xv(ii+1))^2+(Yv(ii)-Yv(ii+1))^2);
56
57 end
58
59 clear Xv Yv
60
61 SP.a_bar   = SP.a - (1 - SP.gamma)*SP.L0;
62 SP.Theta0 = atan((SP.b0)/(SP.a_bar/2)); % Theta0 = initial angle
63
64
65
66
67 \subsection*{Mechanical properties}
68
69
70 %compression SLS model
71 % E_c_r    = (1 - SP.acmp)*E
72 % E_c_v    = SP.acmp*E
73
74 %Torsional SLS model
75 % E_tr_r   = (1 - SP.at)*E
76 % E_tr_v   = SP.at*E
77
78 SP.nuC     = 1.3046e+07; % Damping coefficient compression viscoelastic
79           material
80 SP.ac      = 0.1449;
81 % SP.EC    = 1.2032e+07;% Commented for isometry
82
83 if SP.t == 3/1000
84     SP.E    = 1.2032e+07;
85     % SP.ET = 1.5131e+08;% Commented for isometry
86     SP.nuT  = 3.9554; % Damping coefficient torsion viscoelastic material
87     SP.at   = 0.1621;
88
89 elseif SP.t == 5/1000
90
91     SP.E    = 57691000;
92     % SP.ET = 1.0335e+08; % Commented for isometry
93     SP.nuT  = 10.6406; % Damping coefficient torsion viscoelastic material
94     SP.at   = 0.1558;
95

```

```

96 end
97
98
99
100 \subsection*{Deriving Force – Deformation behaviour}
101
102
103 % Deriving force – deformation
104 VAL = FD_relation(SP,Para);
105
106 % Deriving force – deformation – analytical model
107 VAL2 = FD_analytical(SP);
108
109 % Deriving force – deformation at instant and quasi static speeds
110 ExVAL = FD_Ext2(SP);
111
112
113 ind = islocalmin(VAL.Force);
114 Pos = VAL.Bpos(ind);
115 Vel = Pos/VAL.Time(end);
116
117
118
119 \subsection*{PLots}
120
121
122 figure;
123 plot(VAL.Bpos,VAL.Force,'r',VAL2.d_total_N/1000,VAL2.f_total_N,'.b',...
124      (SP.b0 - ExVAL.iBpos),ExVAL.iForce,'—m',...
125      (SP.b0 - ExVAL.rBpos),ExVAL.rForce,'—k')
126 xlabel('Strain')
127 ylabel('Force')
128 title('Force vs Strain')
129 legend('SLS model','Static analytical model',...
130        'instantaneous deformation','relaxed deformation')
131
132 figure;
133 plot(VAL.Time,VAL.Force)
134 title('Force vs Time')
135 xlabel('Time')
136 ylabel('Force')
137
138
139
140 \subsection*{Recovery time estimation =}
141
142
143 % Force deformation at different time stamps
144 VALConST = ConstStiff_FD(VAL.Stiff(end,:),SP,Para);
145
146 figure;
147 plot(VALConST.B,VALConST.Force)
148 title('Constant Stiff')
149
150 ind = islocalmin(VALConST.Force);
151 Fmin = VALConST.Force(ind);

```

```

152
153 if Fmin < 0
154
155     SZ          = length(VAL.Stiff);
156
157     MinF        = zeros(SZ,1);
158     MinPos      = zeros(SZ,1);
159
160     for k      = SZ:-1:1
161
162         LocalMin    = ConstStiff_FD(VAL.Stiff(k,:),SP,Para);
163         ind         = islocalmin(LocalMin.Force);
164         MinF(k)     = LocalMin.Force(ind);
165         MinPos(k)   = LocalMin.B(ind);
166
167         if MinF(k) > 0
168             break;
169         end
170
171     end
172
173     figure;
174     plot(VAL.Stiff(:,1),MinF)
175     title('Local minima')
176
177     % Initial pos
178     Fsq          = VALConST.Force.^2;
179     ind         = islocalmin(Fsq);
180     Xist_inp     = VALConST.B(ind);
181     ST.Int      = Xist_inp(2);
182
183     % Snap back
184     Fsq          = LocalMin.Force.^2;
185     ind         = islocalmin(Fsq);
186     ST.SnapBk   = LocalMin.B(ind);
187
188     Time        = Recovery(SP,ST);
189     fprintf('\n Recovery time is %d seconds or less\n',Time)
190     fprintf('\n Target strain was set to %d mm\n',Para.ConstStrain*1000)
191
192 end

```

```

1
2 % This LaTeX was auto-generated from MATLAB code.
3 % To make changes, update the MATLAB code and republish this document.
4
5
6
7
8 function [VAL] = FD_relation(SP,Para)
9
10
11 % Stiffness
12
13 SFQ          = [1 1.5 1.65 2 2.314 3].';

```

```

14 CFTM1           = [2.9850 3.0719 3.0994 3.1681 3.2212 3.6687].';
15 CFCM1           = [0.9592 0.96 0.96 0.9675 0.9792 0.8667].';
16
17 CFT              = fit(SFQ,CFTM1,'poly4');
18 CFC              = fit(SFQ,CFCM1,'poly4');
19
20 LocalPara.CFT    = CFT.p1*SP.Q.^4 + CFT.p2*SP.Q.^3 + CFT.p3*SP.Q.^2 ...
21                  + CFT.p4*SP.Q + CFT.p5;
22 LocalPara.CFC    = CFC.p1*SP.Q.^4 + CFC.p2*SP.Q.^3 + CFC.p3*SP.Q.^2 ...
23                  + CFC.p4*SP.Q + CFC.p5;
24
25
26 SF.Kc1           = LocalPara.CFC*(1 - SP.ac)*SP.E*SP.Ar/(SP.gamma*SP.L0/2);
27 SF.Kc2           = LocalPara.CFC*SP.ac*SP.E*SP.Ar/(SP.gamma*SP.L0/2);
28
29 SF.Kt1           = 2*LocalPara.CFT*(1 - SP.at)*SP.E*SP.I/SP.L0;
30 SF.Kt2           = 2*LocalPara.CFT*SP.at*SP.E*SP.I/SP.L0;
31
32 \begin{par}
33 Behaviour of input signal
34 \end{par} \vspace{1em}
35
36 LocalPara.angTr  = atan((SP.b0 - Para.ConstStrain)/(SP.a_bar/2));
37 LocalPara.LTr    = SP.a_bar/(SP.gamma*cos(LocalPara.angTr));
38
39 LocalPara.TmTr   = Para.ConstStrain/Para.P_Vel;
40 LocalPara.TmRx   = Para.RDur + LocalPara.TmTr;
41
42 syms t s Theta
43
44 VAL.PrbPos       = Para.P_Vel*t*(1 - heaviside(t - LocalPara.TmTr)) + ...
45                  Para.ConstStrain*heaviside(t - LocalPara.TmTr);
46
47 matlabFunction(VAL.PrbPos,'file','UpdatePos','vars',t);
48
49 VAL.Xt           = SP.b0 - VAL.PrbPos;
50
51 LocalPara.dt     = LocalPara.TmTr/40000;
52 est.t            = (0:LocalPara.dt:LocalPara.TmTr).';
53 est.b            = SP.b0 - Para.P_Vel*est.t;
54 est.Theta        = atan(2*est.b/SP.a_bar);
55 est.L            = SP.a_bar./(SP.gamma*cos(est.Theta));
56
57 Loptions         = fitoptions('poly2', 'Lower', [-Inf -Inf 0], ...
58                             'Upper', [Inf Inf 0]);
59
60 VAL.Thetat       = ((LocalPara.angTr - SP.Theta0)/LocalPara.TmTr*t)...
61                  *(1 - heaviside(t - LocalPara.TmTr)) + ...
62                  (LocalPara.angTr - SP.Theta0)*...
63                  heaviside(t - LocalPara.TmTr);
64
65 matlabFunction(VAL.Thetat,'file','ThetaUpdate','vars',t);
66
67 est.fitL         = fit(est.t,est.L - SP.L0,'poly2',Loptions);
68 VAL.Lt           = (est.fitL.p1*t^2 + est.fitL.p2*t + est.fitL.p3)*...
69                  (1 - heaviside(t - LocalPara.TmTr)) + ...

```

```

70         (LocalPara.LTr - SP.L0)*heaviside(t - LocalPara.TmTr);
71
72 VAL.fitL      = SP.gamma*[est.fitL.p1;est.fitL.p2;est.fitL.p3]/2;
73
74 matlabFunction(VAL.Lt, 'file', 'LUpdate', 'vars', t);
75
76 VAL.Thetat_1  = VAL.Thetat;
77 VAL.Thetat_2  = 2*VAL.Thetat;
78 VAL.Lt_1      = SP.gamma*(VAL.Lt)/2;
79
80 VAL.ThetaS_1  = laplace(VAL.Thetat_1, t, s);
81 VAL.ThetaS_2  = laplace(VAL.Thetat_2, t, s);
82 VAL.LS_1      = laplace(VAL.Lt_1, t, s);
83
84
85 VAL.FS_tr1    = (SF.Kt1 + s*SF.Kt2/(s + SF.Kt2/SP.nuT))*VAL.ThetaS_1;
86 VAL.FS_tr2    = (SF.Kt1 + s*SF.Kt2/(s + SF.Kt2/SP.nuT))*VAL.ThetaS_2;
87 VAL.FS_Cp     = (SF.Kc1 + s*SF.Kc2/(s + SF.Kc2/SP.nuC))*VAL.LS_1;
88
89 VAL.Ft_tr1    = ilaplace(VAL.FS_tr1, s, t);
90 VAL.Ft_tr2    = ilaplace(VAL.FS_tr2, s, t);
91 VAL.Ft_Cp     = ilaplace(VAL.FS_Cp, s, t);
92
93 VAL.F         = 2*sin(Theta + SP.Theta0)*VAL.Ft_Cp + ...
94               4*cos(Theta + SP.Theta0)^2*VAL.Ft_tr2/SP.a_bar + ...
95               4*cos(Theta + SP.Theta0)^2*VAL.Ft_tr1/SP.a_bar;
96
97 thetaslope   = (LocalPara.angTr - SP.Theta0)/(LocalPara.TmTr);
98
99 VAL.dF1      = jacobian(VAL.F, [Theta, t])*[thetaslope; 1];
100 VAL.dF2     = jacobian(VAL.F, [Theta, t])*[0; 1];
101
102 VAL.TorRatio = (VAL.Ft_tr1/VAL.Thetat_1);
103
104 matlabFunction(VAL.TorRatio, 'file', 'Torstf', 'vars', t);
105
106 VAL.Cmpstf   = (VAL.Ft_Cp/(VAL.Lt_1));
107 matlabFunction(VAL.Cmpstf, 'file', 'Cmpstf', 'vars', t);
108
109 matlabFunction(-VAL.F, 'file', 'Force1', 'vars', [Theta, t]);
110 matlabFunction(-VAL.F, 'file', 'Force2', 'vars', [Theta, t]);
111
112 \begin{par}
113 Evaluation of the Force deformation curve
114 \end{par} \vspace{1em}
115
116 VAL.Time     = linspace(0, LocalPara.TmTr, 500).';
117
118 VAL.Time     = [VAL.Time; linspace(LocalPara.TmTr, LocalPara.TmRx, 500).'];
119
120
121 DataSize    = length(VAL.Time);
122 VAL.Force   = zeros(DataSize, 1);
123 VAL.Theta   = zeros(DataSize, 1);
124 VAL.Bpos    = zeros(DataSize, 1);
125 VAL.Lpos    = zeros(DataSize, 1);

```

```

126 VAL.Stiff          = zeros(DataSize,2);
127
128 VAL.Stiff(1,1)     = SF.Kt1 + SF.Kt2;
129 VAL.Stiff(1,2)     = SF.Kc1 + SF.Kc2;
130
131 for                i = 2:DataSize
132
133     VAL.Bpos(i)     = UpdatePos(VAL.Time(i));
134     VAL.Lpos(i)     = SP.gamma*LUpdate(VAL.Time(i))/2;
135     VAL.Theta(i)    = ThetaUpdate(VAL.Time(i));
136
137     if VAL.Time(i) <= LocalPara.TmTr
138
139         VAL.Force(i)= Force1(VAL.Theta(i),VAL.Time(i));
140     else
141
142         VAL.Force(i)= Force2(VAL.Theta(i),VAL.Time(i));
143     end
144     VAL.Stiff(i,1)  = Torstf(VAL.Time(i));
145     VAL.Stiff(i,2)  = Cmpstf(VAL.Time(i));
146
147 end
148
149 figure;
150 plot(VAL.Time,((max(VAL.Stiff)) - VAL.Stiff)/(max(VAL.Stiff)))
151 title('torsional stiffness')
152
153
154 end

```

```

1
2 % This LaTeX was auto-generated from MATLAB code.
3 % To make changes, update the MATLAB code and republish this document.
4
5
6 \begin{itemize}
7 \setlength{\itemsep}{-1ex}
8   \item Analytical model 2 with higher order terms
9   \item Mode 1
10  \item Mode 3
11 \end{itemize}
12
13 function [VAL] = FD_analytical(SP)
14
15
16
17 \subsection*{Analytical model 2 with higher order terms}
18
19
20 N1      = 2*pi;
21 N3      = 4*pi;
22 dN      = 0.01;
23
24 Del_top = 28/27 - (2*pi*sqrt(1/6 + (16/(81*pi^2)) - 1/SP.Q^2))/3;
25 Del_bot = 28/27 + (2*pi*sqrt(6^-1 + (16/(81*pi^2)) - 1/SP.Q^2))/3;

```

```

26
27 Nr = (0:dN:N3-dN);
28
29
30
31 \subsection*{Mode 1}
32
33
34 syms N Fnu
35
36 Ca      = (3/(16*N^4))*(1+ (tan(N/4))^2/3 - tan(N/4)/(N/4));
37 Cb      = -4*pi^2/(N^2 - 4*pi^2)^2;
38 Cc      = N^2/(12*SP.Q^2) - pi^2*N^2*(N^2 - 8*pi^2)/(4*(N^2 - 4*pi^2)^2);
39
40 Del     = N^2/(N^2 - 4*pi^2) - Fnu*(N/4 - tan(N/4))/N^3;
41
42 F_roots = roots([Ca Cb Cc]);
43
44 matlabFunction(F_roots,'file','Froots');
45 matlabFunction(Del,'file','Delta');
46
47
48 for i = 1:length(Nr)
49
50     check(:,1) = Froots(Nr(i));
51
52     if imag(check(1))||imag(check(2))
53         break;
54     end
55
56     check2(:,1) = Delta(check(:,1),Nr(i));
57
58     if (check2(1)<0)|| (check2(1)>2.2)|| (check2(2)<0)|| (check2(2)>2.2)
59         continue;
60     end
61     Fr_val(:,i)    = check(:,1);
62     Del_val(:,i)   = check2(:,1);
63
64 end
65
66
67
68 \subsection*{Mode 3}
69
70
71 % axial force = N4
72
73 if SP.Q >= 2.3141
74     Del3 = (Del_top:0.0001:Del_bot);
75
76     F3    = 64*pi^2*(4/3 - Del3);
77
78     VAL.f_total_N    = [Fr_val(1,2:end),Fr_val(2,2:end),F3]*...
79         SP.E*SP.I*SP.Q*SP.t/(SP.a)^3;
80     VAL.d_total_N    = [Del_val(1,2:end),Del_val(2,2:end),Del3]*...
81         SP.Q*SP.t*1000;

```



```

82
83 else
84     VAL.f_total_N = [Fr_val(1,2:end),Fr_val(2,2:end)]*...
85                     SP.E*SP.I*SP.Q*SP.t/(SP.a)^3;
86     VAL.d_total_N = [DeL_val(1,2:end),DeL_val(2,2:end)]*...
87                     SP.Q*SP.t*1000;
88
89 end
90
91
92 end

```

```

1
2 % This LaTeX was auto-generated from MATLAB code.
3 % To make changes, update the MATLAB code and republish this document.
4
5
6
7 \begin{itemize}
8 \setlength{\itemsep}{-1ex}
9 \item Spring deformation
10 \item Evaluation of the Force deformation curve
11 \end{itemize}
12
13 function [VAL] = FD_Ext2(SP)
14
15
16 % Stiffness
17
18 SFQ = [1 1.5 1.65 2 2.314 3].';
19 CFTM1 = [2.9850 3.0719 3.0994 3.1681 3.2212 3.6687].';
20 CFCM1 = [0.9592 0.96 0.96 0.9675 0.9792 0.8667].';
21
22 CFT = fit(SFQ,CFTM1,'poly4');
23 CFC = fit(SFQ,CFCM1,'poly4');
24
25 LocalPara.CFT = CFT.p1*SP.Q.^4 + CFT.p2*SP.Q.^3 + CFT.p3*SP.Q.^2 ...
26               + CFT.p4*SP.Q + CFT.p5;
27 LocalPara.CFC = CFC.p1*SP.Q.^4 + CFC.p2*SP.Q.^3 + CFC.p3*SP.Q.^2 ...
28               + CFC.p4*SP.Q + CFC.p5;
29
30 SF.Kc1 = LocalPara.CFC*(1 - SP.ac)*SP.E*SP.Ar/(SP.gamma*SP.L0/2);
31 SF.Kc2 = LocalPara.CFC*SP.ac*SP.E*SP.Ar/(SP.gamma*SP.L0/2);
32
33 SF.Kt1 = 2.0*LocalPara.CFT*(1 - SP.at)*SP.E*SP.I/SP.L0;
34 SF.Kt2 = 2.0*LocalPara.CFT*SP.at*SP.E*SP.I/SP.L0;
35
36 \begin{par}
37 reaction force
38 \end{par} \vspace{1em}
39
40 VAL.dTheta = 2*SP.Theta0/399;
41
42 syms Theta L b
43

```

```

44 X(1,1) = SP.gamma*L*cos(Theta)/2 - SP.a_bar/2;
45 X(2,1) = SP.gamma*L*sin(Theta)/2 - b;
46
47 q = [L b];
48
49 LocalPara.A = jacobian(X,q);
50 LocalPara.B = jacobian(-X,Theta);
51 LocalPara.VEL = LocalPara.A\LocalPara.B;
52
53
54
55 \subsection*{Spring deformation}
56
57
58 % instantaneous deformation
59
60 SF.Mu(1,1) = Theta - SP.Theta0;
61 SF.Mu(2,1) = SP.gamma*(L - SP.L0)/2;
62 SF.Mu(3,1) = (pi-2*Theta) - (pi-2*SP.Theta0);
63 SF.Mu(4,1) = SP.gamma*(L - SP.L0)/2;
64 SF.Mu(5,1) = Theta - SP.Theta0;
65
66 K1 = SF.Kt1 + SF.Kt2; % torsion stiffness
67 K2 = SF.Kc1 + SF.Kc2; % compression stiffness
68 SF.SMatrix = [K1 K2 K1 K2 K1];
69
70 SF.Mu = SF.SMatrix*SF.Mu.^2/2;
71 dPE = simplify(jacobian(SF.Mu,[Theta,L,b])*...
72 [1;LocalPara.VEL(1,1);LocalPara.VEL(2,1)]);
73
74 VAL.iF = dPE/(jacobian(b-SP.b0,b)*...
75 LocalPara.VEL(2,1));
76
77 VAL.idF = simplify(jacobian(VAL.iF,[Theta,L,b])*...
78 [1;LocalPara.VEL(1,1);LocalPara.VEL(2,1)])*VAL.dTheta;
79
80 matlabFunction(VAL.idF,'file','ExtiForce','vars',[Theta,L]);
81
82 % relaxed deformation
83
84 SF.Mu(1,1) = Theta - SP.Theta0;
85 SF.Mu(2,1) = SP.gamma*(L - SP.L0)/2;
86 SF.Mu(3,1) = (pi-2*Theta) - (pi-2*SP.Theta0);
87 SF.Mu(4,1) = SP.gamma*(L - SP.L0)/2;
88 SF.Mu(5,1) = Theta - SP.Theta0;
89
90 K1 = SF.Kt1; % torsion stiffness
91 K2 = SF.Kc1; % compression stiffness
92 SF.SMatrix = [K1 K2 K1 K2 K1];
93
94 SF.Mu = SF.SMatrix*SF.Mu.^2/2;
95 dPE = simplify(jacobian(SF.Mu,[Theta,L,b])*...
96 [1;LocalPara.VEL(1,1);LocalPara.VEL(2,1)]);
97
98 VAL.rF = dPE/(jacobian(b-SP.b0,b)*...
99 LocalPara.VEL(2,1));

```

```

100
101 VAL.rdF          = simplify(jacobian(VAL.rF,[Theta,L,b])*...
102                [1;LocalPara.VEL(1,1);LocalPara.VEL(2,1)])*VAL.dTheta;
103
104
105 matlabFunction(VAL.rdF,'file','ExtrForce','vars',[Theta,L]);
106
107
108
109 \subsection*{Evaluation of the Force deformation curve}
110
111
112 DataSize          = 400;
113 VAL.Theta         = linspace(SP.Theta0,-SP.Theta0,DataSize).';
114
115 VAL.iForce        = zeros(DataSize,1);
116 VAL.iBpos         = zeros(DataSize,1);
117 VAL.iLpos         = zeros(DataSize,1);
118
119 VAL.rForce        = zeros(DataSize,1);
120 VAL.rBpos         = zeros(DataSize,1);
121 VAL.rLpos         = zeros(DataSize,1);
122
123 VAL.iBpos(1)      = SP.b0;
124 VAL.rBpos(1)      = SP.b0;
125
126 VAL.iLpos(1)      = SP.L0;
127 VAL.rLpos(1)      = SP.L0;
128
129 for               i = 2:DataSize
130
131     VAL.iBpos(i)   = tan(VAL.Theta(i))*SP.a_bar/2;
132     VAL.iLpos(i)   = SP.a_bar/(SP.gamma*cos(VAL.Theta(i)));
133
134     VAL.iForce(i,1) = ExtiForce(VAL.Theta(i,1),VAL.iLpos(i,1))...
135         + VAL.iForce(i-1,1);
136
137     VAL.rBpos(i)   = tan(VAL.Theta(i))*SP.a_bar/2;
138     VAL.rLpos(i)   = SP.a_bar/(SP.gamma*cos(VAL.Theta(i)));
139
140     VAL.rForce(i,1) = ExtrForce(VAL.Theta(i,1),VAL.rLpos(i,1))...
141         + VAL.rForce(i-1,1);
142
143 end
144
145
146 end

```

```

1
2 % This LaTeX was auto-generated from MATLAB code.
3 % To make changes, update the MATLAB code and republish this document.
4
5
6 \begin{itemize}
7 \setlength{\itemsep}{-1ex}

```

```

8     \item Energy
9     \end{itemize}
10
11     function [VALConST] = ConstStiff_FD(Stiff,SP,Para)
12
13
14     SP.dTheta          = 1/500;
15
16     LocalPara.angTr    = atan((SP.b0 - Para.ConstStrain)/(SP.a_bar/2));
17     LocalPara.LTr      = SP.a_bar/(SP.gamma*cos(LocalPara.angTr));
18
19
20     syms Theta L B
21
22     CAL.X(1)           = SP.gamma*L*cos(Theta)/2 - SP.a_bar/2;
23     CAL.X(2)           = SP.gamma*L*sin(Theta)/2 - B;
24
25     CAL.q              = [L B];
26
27     CAL.A              = jacobian(CAL.X,CAL.q);
28     CAL.B              = jacobian(-CAL.X,Theta);
29     CAL.Rate           = CAL.A\CAL.B;
30
31
32
33     \subsection*{Energy}
34
35
36     CAL.Mu(1,1)        = Theta - SP.Theta0;
37     CAL.Mu(2,1)        = SP.gamma*(L - SP.L0)/2;
38     CAL.Mu(3,1)        = (pi - 2*Theta) - (pi - 2*SP.Theta0);
39     CAL.Mu(4,1)        = SP.gamma*(L - SP.L0)/2;
40     CAL.Mu(5,1)        = Theta - SP.Theta0;
41
42     CAL.SMatrix        = [Stiff(1) Stiff(2) Stiff(1) Stiff(2) Stiff(1)];
43
44     CAL.PE             = CAL.SMatrix*CAL.Mu.^2/2;
45     CAL.F              = simplify(jacobian(CAL.PE,[Theta,L,B])*...
46         [1;CAL.Rate(1);CAL.Rate(2)]);
47     CAL.F              = simplify(CAL.F/(jacobian(B-SP.b0,B)*...
48         CAL.Rate(2,1)));
49
50     CAL.dF             = simplify(jacobian(CAL.F,[Theta,L,B])*...
51         [1;CAL.Rate(1);CAL.Rate(2)]*SP.dTheta);
52
53     matlabFunction(CAL.dF,'file','Con_FD','vars',[Theta,L]);
54
55
56     VALConST.Theta     = (SP.Theta0:-SP.dTheta:LocalPara.angTr).';
57
58     VALConST.Force     = zeros(size(VALConST.Theta));
59     VALConST.L         = zeros(size(VALConST.Theta));
60     VALConST.B         = zeros(size(VALConST.Theta));
61
62     VALConST.L(1)      = SP.L0;
63

```

```

64 for i = 2: length(VALConST.Theta)
65
66     VALConST.L(i,1)    = (SP.a_bar)/(SP.gamma*cos(VALConST.Theta(i,1)));
67     VALConST.B(i,1)    = SP.b0 - SP.a_bar*tan(VALConST.Theta(i,1))/2;
68
69     VALConST.Force(i,1)= Con_FD(VALConST.Theta(i,1),VALConST.L(i,1)) + ...
70                             VALConST.Force(i - 1,1);
71
72 end
73
74
75 end

```

```

1
2 % This LaTeX was auto-generated from MATLAB code.
3 % To make changes, update the MATLAB code and republish this document.
4
5
6
7 function [Time] = Recovery(SP,ST)
8 % Stiffness
9 SFQ          = [1 1.5 1.65 2 2.314 3].';
10 CFTM1        = [2.9850 3.0719 3.0994 3.1681 3.2212 3.6687].';
11 CFCM1        = [0.9592 0.96 0.96 0.9675 0.9792 0.8667].';
12
13 CFT          = fit(SFQ,CFTM1,'poly4');
14 CFC          = fit(SFQ,CFCM1,'poly4');
15
16 LocalPara.CFT = CFT.p1*SP.Q.^4 + CFT.p2*SP.Q.^3 + CFT.p3*SP.Q.^2 ...
17                 + CFT.p4*SP.Q + CFT.p5;
18 LocalPara.CFC = CFC.p1*SP.Q.^4 + CFC.p2*SP.Q.^3 + CFC.p3*SP.Q.^2 ...
19                 + CFC.p4*SP.Q + CFC.p5;
20
21 SF.Kc1       = LocalPara.CFC*(1 - SP.ac)*SP.E*SP.Ar/(SP.gamma*SP.L0/2);
22 SF.Kc2       = LocalPara.CFC*SP.ac*SP.E*SP.Ar/(SP.gamma*SP.L0/2);
23
24 SF.Kt1       = 2*LocalPara.CFT*(1 - SP.at)*SP.E*SP.I/SP.L0;
25 SF.Kt2       = 2*LocalPara.CFT*SP.at*SP.E*SP.I/SP.L0;
26
27 ST.SBAng     = SP.Theta0 - atan((SP.b0 - ST.SnapBk)/(SP.a_bar/2));
28 ST.IntAng    = SP.Theta0 - atan((SP.b0 - ST.Int)/(SP.a_bar/2));
29
30 Time        = -log(ST.SBAng/ST.IntAng)*(1 + SF.Kt1/SF.Kt2)*...
31                 (SP.nuT/SF.Kt1);
32 end

```



# Bibliography

- [1] Nucleation in Condensed Matter: Applications in Materials and Biology. In K F Kelton and A L Greer, editors, Nucleation in Condensed Matter, volume 15 of Pergamon Materials Series, page iii. Pergamon, 2010. doi: [https://doi.org/10.1016/S1470-1804\(09\)01521-1](https://doi.org/10.1016/S1470-1804(09)01521-1). URL <http://www.sciencedirect.com/science/article/pii/S1470180409015211>.
- [2] ASTM. Standard Test Method for Tensile Properties of Plastics, 14.
- [3] ASTM. Standard Test Method for Flexural Properties of Polymer Matrix Composite Materials, 15.
- [4] ASTM. Standard Test Methods of Compression Testing of Metallic Materials at Room Temperature, 19.
- [5] A Brinkmeyer, M Santer, A Pirrera, and P M Weaver. Pseudo-bistable self-actuated domes for morphing applications. *International Journal of Solids and Structures*, 49(9):1077–1087, 2012. ISSN 0020-7683. doi: <https://doi.org/10.1016/j.ijsolstr.2012.01.007>. URL <http://www.sciencedirect.com/science/article/pii/S0020768312000170>.
- [6] A Brinkmeyer, A Pirrera, M Santer, and P M Weaver. Pseudo-bistable pre-stressed morphing composite panels. *International Journal of Solids and Structures*, 50(7):1033–1043, 2013. ISSN 0020-7683. doi: <https://doi.org/10.1016/j.ijsolstr.2012.11.019>. URL <http://www.sciencedirect.com/science/article/pii/S0020768312004908>.
- [7] Babak Haghpanah, Ladan Salari-Sharif, Peyman Pourrajab, Jonathan Hopkins, and Lorenzo Valdevit. Multistable Shape-Reconfigurable Architected Materials. *Advanced Materials*, 28(36):7915–7920, 2016. doi: [10.1002/adma.201601650](https://doi.org/10.1002/adma.201601650). URL <https://onlinelibrary.wiley.com/doi/abs/10.1002/adma.201601650>.
- [8] Brian Jensen. Modeling of Large Deflection Members, chapter 4, pages 45–54. John Wiley & Sons, Ltd, 2013. ISBN 9781118516485. doi: [10.1002/9781118516485.ch4](https://doi.org/10.1002/9781118516485.ch4). URL <https://onlinelibrary.wiley.com/doi/abs/10.1002/9781118516485.ch4>.
- [9] Brian Jensen. Modeling of Large Deflection Members, chapter 4, pages 45–54. John Wiley & Sons, Ltd, 2013. ISBN 9781118516485. doi: [10.1002/9781118516485.ch4](https://doi.org/10.1002/9781118516485.ch4). URL <https://onlinelibrary.wiley.com/doi/abs/10.1002/9781118516485.ch4>.
- [10] Jin Qiu, J H Lang, and A H Slocum. A curved-beam bistable mechanism. *Journal of Microelectromechanical Systems*, 13(2):137–146, apr 2004. doi: [10.1109/JMEMS.2004.825308](https://doi.org/10.1109/JMEMS.2004.825308).
- [11] Armin Kibele, Claudia Classen, Thomas Muehlbauer, Urs Granacher, and David G Behm. Metastability in plyometric training on unstable surfaces: a pilot study. *BMC sports science, medicine & rehabilitation*, 6:30, jul 2014. ISSN 2052-1847. doi: [10.1186/2052-1847-6-30](https://doi.org/10.1186/2052-1847-6-30). URL <https://www.ncbi.nlm.nih.gov/pubmed/25089202><https://www.ncbi.nlm.nih.gov/pmc/articles/PMC4118276/>.
- [12] Armin Kibele, Urs Granacher, Thomas Muehlbauer, and David G Behm. Stable, Unstable and Metastable States of Equilibrium: Definitions and Applications to Human Movement. *Journal of sports science & medicine*, 14(4):885–887, nov 2015. ISSN 1303-2968. URL <https://www.ncbi.nlm.nih.gov/pubmed/26664288><https://www.ncbi.nlm.nih.gov/pmc/articles/PMC4657434/>.
- [13] Craig Lusk. Using Pseudo-Rigid Body Models, chapter 5, pages 55–76. John Wiley & Sons, Ltd, 2013. ISBN 9781118516485. doi: [10.1002/9781118516485.ch5](https://doi.org/10.1002/9781118516485.ch5). URL <https://onlinelibrary.wiley.com/doi/abs/10.1002/9781118516485.ch5>.

- [14] Raphaël Morillon, David Liénard, Maarten J Chrispeels, and Jean-Paul Lassalles. Rapid Movements of Plants Organs Require Solute-Water Cotransporters or Contractile Proteins. *Plant Physiology*, 127(3):720–723, 2001. ISSN 0032-0889. doi: 10.1104/pp.010732. URL <http://www.plantphysiol.org/content/127/3/720>.
- [15] Xin Ren, Raj Das, Phuong Tran, Tuan Duc Ngo, and Yi Min Xie. Auxetic metamaterials and structures: a review. *Smart Materials and Structures*, 27(2):23001, jan 2018. doi: 10.1088/1361-665x/aaa61c. URL <https://doi.org/10.1088/1361-665x/aaa61c>.
- [16] Sicong Shan, Sung H Kang, Jordan R Raney, Pai Wang, Lichen Fang, Francisco Candido, Jennifer A Lewis, and Katia Bertoldi. Multistable Architected Materials for Trapping Elastic Strain Energy. *Advanced Materials*, 27(29):4296–4301, 2015. doi: 10.1002/adma.201501708. URL <https://onlinelibrary.wiley.com/doi/abs/10.1002/adma.201501708>.
- [17] J L Synge. *Principles Of Mechanics*. Read Books Limited, 2011. ISBN 9781446545614. URL <https://books.google.nl/books?id=fTR8CgAAQBAJ>.
- [18] Hang Yang and Li Ma. Multi-stable mechanical metamaterials by elastic buckling instability. *Journal of Materials Science*, 54(4):3509–3526, feb 2019. ISSN 1573-4803. doi: 10.1007/s10853-018-3065-y. URL <https://doi.org/10.1007/s10853-018-3065-y>.